Scientific paper

Recycling of Waste Incineration Bottom Ash and Heavy Metal Immobilization by Geopolymer Production

Zhuguo Li[1*], Ryusei Kondo[2] and Ko Ikeda[3]

Received 4 February 2021, accepted 23 March 2021 doi:10.3151/jact.19.259

Abstract

Municipal waste incineration ash contains heavy metals, and the safety of its disposal and reuse is an important issue. In this study, we discussed a safe recycling technology for bottom ash (BA) by utilizing the excellent heavy metal immobilization feature of geopolymer (GP). First, the differences in chemical compositions, physical properties, and heavy metal contents of BAs discharged in different months were investigated. Next, the reaction products and strength of the mixture of BA and alkali-activator (AA) solution were examined to clarify the reactivity of BA in the AA solution. We also investigated the effects of the discharge time of BA, ingredients of AA solution, curing method and mixing ratio of BFS on the setting time, strength and heavy metal immobilization capacity of GP mortar using ground granulated blast furnace slag (BFS) and coal fly ash (CFA) as precursors, and BA as fine aggregate, and discussed reaction products and micro-structure of the GP mortar. The main results are as follows: 1) BA contained a small amount of amorphous phase. Hardened GP monolith using BA and AA solution was not dense and had a very low strength. 2) The BFS/CFA-based GP mortar with BA as fine aggregate had a higher strength and a longer setting time when sodium silicate solution (WG) was used as AA solution than when sodium hydroxide was added or used entirely. The GP mortars using the BAs discharged in the warm season had longer setting time and higher strength. The reaction products of the GP mortar with WG solution and BA were mainly C-A-S-H gels. The leaching of heavy metal elements (HME) from the GP mortars increased with decreasing the alkalinity of leachate, but the effect of BA's discharge season was not found in this study. The HME leaching concentrations from the GP mortars in non-acidic water environment were less than the HME leaching limits specified for recycled construction materials directly contacting with water, thus the GP materials with BA can be used in dry or non-acidic water environment. However, when used in acidic water environment, the BA content in the GP materials should be reduced.

1. Introduction

With the rapid economic development and the growth in population, the consumption of resources and energy has been increasing worldwide. As a result, natural resources become scarce and wastes have been generated increasingly, making waste disposal to be a global problem. In order to realize a sustainable society, it is necessary to reduce waste generation, promote recycling, and ensure safe disposal. In Japan, total amount of general waste (municipal solid waste, MSW) has been on a slight downward trend since fiscal 2011, but total MSW discharged in fiscal 2018 was still high at 42.72 million tons (MEJ 2020). Incineration is a viable method to reduce MSW's volume by 85-90% (Hjelmer 1996) and to recover energy, thus it has become a global trend in waste management, especially in land scarce cities as it mitigates the need of landfill. In fiscal year 2018, the MSW incineration rate was 80.1%, and the weight reduction rate of MSW was 79.2% in Japan (MEJ 2020).

There are several different types of incinerators, which are broadly divided into two categories: incinerator and melting furnace. The former burns solid waste, such as stoker type incinerator and fluidized-bed incinerator, the latter, however, only melts incineration ash, or burn solid waste and melt the incineration ash in a combined process, including ash melting furnace, direct melting furnace, and gasification-melting furnace, etc. The stoker type incinerator discharges bottom ash (BA) and fly ash (MSWI-FA), while the fluidized-bed incinerator mainly generates fly ash (FBI-FA) collected by bug filters. On the other hand, melting furnaces discharge slag and melting fly ash (M-FA). The BA accounts nearly 90%, and the remaining 10% are MSWI-FA collected from the air pollution control treatment system (Kamada 2016). BA, MSWI-FA and M-FA contain more chlorine and heavy metals, such as Cd, Cu, Pb, As, Cr, Zn, and Se, etc., though heavy metals in the BA are less than those in the MSWI-FA and the M-FA. Leaching of toxic substances from BA and fly ashes is potentially harmful to the water and soil environments, and has become a great environmental concern with respect to the disposal and/or reuse of incineration residues. However, heavy metals

[1]Professor, Graduate School of Sciences and Technology for Innovation, Yamaguchi University, Ube, Japan.
*Corresponding author, *E-mail*: li@yamaguchi-u.ac.jp
[2]Master's course student, Graduate School of Sciences and Technology for Innovation, Yamaguchi University, Ube, Japan.
[3]Professor Emeritus, Graduate School of Sciences and Technology for Innovation, Yamaguchi University, Ube, Japan.

are not easily leached from the slag produced by the melting furnaces, because they are immobilized in the network structure formed by silica (SiO_2), which is a main component of slag. Thus, the slag has been recycled as roadbed material and concrete aggregate. At present, in Japan stoker type incinerators, fluidized-bed incinerators and gasification melting furnaces burn 75%, 12%, and 14% of MSW by weight, respectively (Sakanakura 2019). Hence, a very large amount of BA is discharged.

Since it is difficult to increase landfill sites, there have been significant efforts in several research areas to valorize BA rather than sending it to landfill. At present, in Japan there are two main methods of recycling BA: 1) melting BA in a melting furnace to produce slag used as aggregates of asphalt concrete for road construction and cement-based concrete, and 2) using BA as a raw material for cement clinker. However, melting BA needs much energy. In developed countries like Japan, there will be less road construction, and due to the presence of free CaO in the slag, the pop-out phenomenon was observed in the concrete using the melting slag as an alternative to natural sand (Ikeda *et al.* 2009). Therefore, the use of melting slags is stagnant so that much of them are used as covering soil for landfill, and embankment fill material, etc. On the other hand, when using BA as raw material for cement clinker, it must be washed to remove chlorine (Cl), and pre-treated for heavy metal recovery such as Cr. For ensuring cement quality and not reducing the sintering efficiency of cement clinker, the BA replaces a very small portion (about 0.5-1%) of clinker's virgin raw materials, thus the BA recycling rate remains low in Japan (Sakanakura 2019). In addition, uneven distribution of cement plants leads to high transportation cost of BA. Currently, BA is also used as partial or integral natural aggregate substitute for producing cementitious materials (Kuo *et al.* 2013), but costly pre-treatment for removing heavy metals is generally required beforehand, or stockpiling outdoors is done for a period to allow carbonation for reducing the mobility of hazardous elements (Arickx *et al.* 2010), called previous weathering stabilization (Giro-Paloma *et al.* 2017). Nevertheless, it is also necessary to keep in mind the leaching behavior of remained heavy metals from the recycled materials in the environments with different pH values. Therefore, reuse of BA is greatly restricted due to its high content in heavy metals.

Geopolymer (GP) is a synthetic alkali-aluminosilicate binder formed through a reaction of aluminosilicate powder in alkaline solution. It comprises of tetrahedral silicate and aluminate units linked in three-dimensional structure by covalent bonds, with negative charges associated with tetrahedral Al^{3+} charge-balanced by alkali cations. Starting materials essential for the GP formation consists of two main parts: reactive aluminosilicate and alkali activator (AA) solution. Reactive aluminosilicate is typically derived from metakaolin or industrial by-products such as coal fly ash (CFA), and AA solution is commonly alkali metal hydroxide and/or silicate solution. Initially GP was produced by using metakaolin (Davidovits 2015), but recently, many researches have used both ground granulated blast furnace slag (BFS) and CFA as precursors in terms of waste utilization and strength development of GP (Li and Li 2018). The CO_2 emissions of concrete with BFS/CFA-based GP binder are 40-60% of Portland cement concrete, under the condition that two kinds of concrete have almost the same slump and compressive strength (Li 2016a). The melting slag of MSW incineration ash has also been used to produce geopolymers (Li *et al.* 2013; Yamaguchi *et al.* 2013). However, due to the presence of metallic aluminum in melting slag, geopolymer adding the melting slag powder foams and expands. Li and Ikeda (2018) have taken advantage of this foaming characteristic to develop a technology of foamed geopolymer.

Geopolymer is excellent at immobilizing heavy metals and radioactive elements by physical encapsulation and stable chemical bond in GP matrices (Vempati *et al.* 1995; Li *et al.* 2018), providing a safe way to recycle hazardous wastes. It has been confirmed that GP can immobilize heavy metals contained in MSWI-FA by using the MSWI-FA as a precursor of GP (Tome *et al.* 2018). Also, Kondo *et al.* (2020) reported that GP can almost completely immobilize volatile organic compounds of BA, such as toluene, octane, 2,4-dimethylheptane, 2,2,4,6,6-pentamethylheptane, decane, and dodecane, and the emission of 2-ethyl-1-hexanol is greatly reduced from the GP using BA. With the increasing interest of safe recycling of BA, there have been attempts to use ground BA as sole precursor or mix BA together with precursor, since it is normally aluminosilicate (Jo *et al.* 2006; Lee *et al.* 2012; Maldonado-Alameda *et al.* 2020; Zhu *et al.* 2016). This would create a solid material, which can replace other conventional construction products, and it would also result in a greater immobilization of hazardous elements typically found in BA. Previous study (Maldonado-Alameda *et al.* 2020) has revealed that BA is mainly composed of SiO_2, Al_2O_3, and CaO, which are the essential ingredients required to formulate GP. However, its composition varies with particle size fraction, and the availability of reactive phases in each fraction varies as a function of its compositions and the AA concentration. When ground BA is used as sole precursor, BA-based GP has a very low compressive strength (around 3 MPa) (Zhu *et al.* 2016). Chen *et al.* (2016) used BA to produce the aerated geopolymer, which had small dry density (<1.0) and small compressive strength (<3.0 MPa), while had a low heavy metal leaching, satisfying most of the limits of drinking water standard. The GP using BA and BFS as precursors showed a high strength, the use of BA (70%) and BFS (30%) precursors and Na_2SiO_3 (60%) and K_2SiO_3 (40%) solution produced the GP mixes to have 7-day compressive strengths over 50 MPa (Lee *et al.* 2012). Gao *et al.* (2017) produced BFS-based GP mortar by adding the BA with the particles lower than 2 mm to replace 10 to 40% of natural sand. Although the BA adversely affects the strength of

Table 1 Chemical compositions, density and fineness modulus of bottom ashes.

BA	23/'19	6/'19	8/'19	10/'19	12/'19	2/'20	5/'20
Discharge time	Feb., Mar. 2019	Jun. 2019	Aug. 2019	Oct. 2019	Dec. 2019	Feb. 2020	May 2020
Physical properties							
Density (g/cm^3)	2.05	1.95	2.13	2.14	1.96	2.03	2.15
Fineness modulus	2.98	2.87	2.51	2.76	3.30	2.93	3.03
Chemical compositions (mass %)							
SiO_2	25.88	40.26	31.12	40.06	26.69	26.96	38.68
TiO_2	1.33	1.50	1.71	1.58	1.58	1.62	1.55
Al_2O_3	15.29	15.96	17.79	16.03	16.90	15.99	16.82
Fe_2O_3	8.03	4.24	5.23	4.77	8.76	12.23	6.38
MnO	0.21	0.14	0.31	0.22	0.36	0.21	0.24
CaO	37.55	24.70	30.00	23.96	32.41	29.59	23.23
MgO	1.51	1.68	1.93	1.89	1.89	2.05	1.76
Na_2O	3.22	3.88	4.47	4.17	3.29	3.40	3.71
K_2O	1.61	2.49	1.76	2.22	1.41	1.34	2.25
P_2O_5	2.63	3.30	2.69	2.87	3.38	3.88	2.47
SO_3	0.55	0.34	0.42	0.39	0.70	0.70	0.64
Cl	1.15	0.64	0.71	0.66	1.06	0.82	0.61
Trace elements	1.03	0.88	1.86	1.19	1.57	1.20	1.66
Total	99.99	100.01	100.00	100.01	100.00	99.99	100.00

the GP mortar due to its porous structure, the GP mortar with 40% BA substitution has a compressive strength of more than 38 MPa, and the leaching of the heavy metals was less, which meets the Dutch legislation.

Using geopolymer technology, it is possible to recycle MSW bottom ash safely to produce construction materials such as blocks, boards, plastering materials and concrete if coarse aggregate is used in addition. However, the physical properties and the chemical compositions of BA depend on the discharge region and period. The influencing factors of BA-based GP's properties such as setting time and strength are not clear. In addition, the leaching of heavy metals from GP with BA should be different from the environments with different pH values. Therefore, in this study, for the practical application of GP technology in BA recycling, we first investigated the reactivity of BA in AA solution by strength test and chemical analysis, then examined the fabrication method and the properties of BFS/CFA-based GP mortar using the BA as fine aggregate, which was discharged from a stoker type MSW incinerator in different months, as well as the immobilization capacity of heavy metals of the GP mortars in acid, neutral and alkaline water environments. Moreover, the microstructure and reaction products of GP mortars with the BA were discussed in detail by X-ray diffraction (XRD) and scanning electron microscope (SEM).

This paper is an extended and enhanced version of the work : [Kondo, R., Li, Z. and Ikeda, K., (2020). "Recycling and heavy metal immobilization of waste incineration ash by geopolymer production" In: *Proceedings of ConMat'20, The 6th International Conference on Concrete Materials - Performance, Innovations, and Structural Implications*, Fukuoka, Japan 27-29 August 2020. Tokyo: Japan Concrete Institute, Paper No. 3-2_2, 877-886.], which has been reported earlier.

2. Materials and test methods

2.1 Municipal solid waste incineration bottom ash (BA)

The bottom ash (BA) samples were collected from the same municipal solid waste incineration facility in Feb. (2/'19), Mar. (3/'19), Jun. (6/'19), Aug. (8/'19), Oct. (10/'19) and Dec. (12/'19) 2019, and Feb. (2/'20) and May (5/'20) 2020, respectively. Since the two BA samples, gathered in Feb. and Mar. 2019, were not enough, they were mixed and used as one sample (23/'19). Before using the BAs, they were screened with a sieve having a mesh size of 4.75 mm to remove coarse residues, and prepared in saturated surface-dry state. The saturated surface-dry state can avoid AA solution being absorbed, which reduces the fluidity of the GP and increases the GP cost, or being diluted by the surface water of BA, which reduces the AA concentration.

Tables 1 and **2** show the chemical compositions, density, and fineness modulus, and **Fig. 1** shows the particle size distribution curves of the BA samples. The chemical compositions were determined by X-ray fluorescence spectroscopy (XRF). The BA mainly contains CaO, SiO_2, Al_2O_3, Fe_2O_3, Na_2O/K_2O, and chlorine (Cl), etc. Many

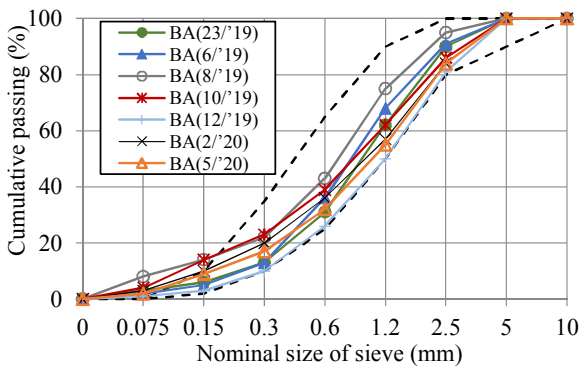

Fig. 1 Particle size distribution of bottom ashes.

Table 2 Trace elements in the bottom ashes (ppm).

Element	23/'19	6/'19	8/'19	10/'19	12/'19	2/'20	5/'20
F	ND	ND	1800	ND	ND	ND	ND
Cr	447	299	660	367	563	402	803
Co	ND	51	55	ND	131	53	45
Ni	112	94	189	129	222	126	142
Cu	1151	932	2540	1865	2793	1993	3074
Zn	3628	2895	5707	3639	5266	3717	5164
Ga	ND	ND	ND	18	ND	23	25
Rb	75	74	49	65	40	34	68
Sr	697	491	558	512	598	604	488
Y	109	ND	124	ND	124	130	106
Zr	80	101	104	78	96	103	125
Nb	ND	17	ND	20	ND	ND	ND
Sn	162	164	362	155	232	192	374
Sb	ND	ND	159	115	161	113	150
Ba	1396	1628	2123	2050	1818	1888	2256
Pb	557	481	837	741	777	409	722
Th	ND	ND	282	49	ND	ND	ND

[Note] ND: Not detectable (i.e., concentration was too small to be detected by XRF analysis).

heavy metal elements were detected, including Cr, Cu, Zn, Pb, etc., the Zn content was particularly large. It was also found that the chemical compositions varied with the time of discharge. The BA samples collected in the cold season (Dec.-Feb.) contained more CaO and chlorine, but less SiO_2. Conversely, in the BA samples collected in the warm season (May-Oct.), there were less CaO and chlorine, but more SiO_2. The Al_2O_3 content in the BA samples was stable, almost independent on the discharge time. Na_2O and K_2O contents were the highest in the BA samples discharged in Aug.-Oct. However, there is no effect of BA discharge time on the contents of heavy metals.

Density and particle size also varied with the discharge time of the BA samples. Compared to the BAs discharged in the cold season (Dec.-Feb.), the densities of the BA samples collected in Aug.-Oct. were larger, and the particles were slightly finer in the whole. According to **Fig. 1**, the content of coarse particles in the size range of 2.5 to 5.0 mm was the largest at 19% in the 12/'19 BA sample, but the 10/'19 and 8/'19 BA samples contained many fine particles smaller than 0.315 mm. However, the size distribution curves of all BA samples fell within the standard distribution range of the size of fine aggregate according to JASS 5, the Japanese Architectural Standard Specification for Reinforced Concrete Work. This range of distribution is the area within the two dashed lines in **Fig. 1**.

Figure 2 shows the XRD patterns for the BA samples.

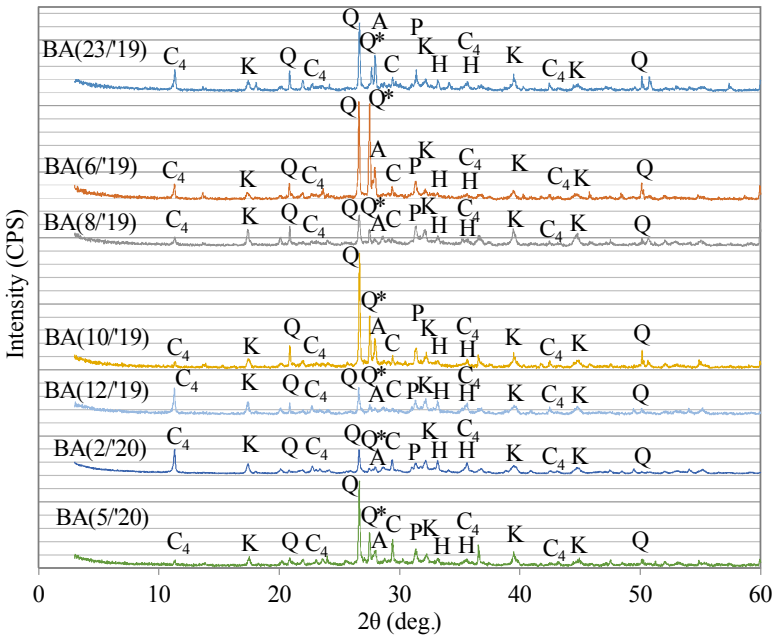

[Notes] Q: Quartz, SiO_2; Q*: Quartz-HP, SiO_2; C: Calcite, $CaCO_3$; A: Anorthite, $CaAl_2Si_2O_8$; K: Katoite, $Ca_3Al_2(OH)_{12}$; H: Hematite, Fe_2O_3; P: Anhydrite, $CaSO_4$; C_4: Hydrotalcite, $Ca_4Al_2O_6Cl_2{\cdot}10H_2O$.

Fig. 2 XRD patterns of bottom ashes.

Although the peak intensity was different from the BA samples for the same crystal compound, the same crystal compounds were confirmed regardless of the discharge time, which were quartz, anorthite, calcite, katoite, hematite, anhydrite, and hydrotalcite (C4). The C4 was rich in the 23/'19, 12/'19, 2/'20 BA samples, but less in the 10/'19 BA sample. The 23/'19, 6/'19, 10/'19, 5/'20 BA samples contained a large amount of quartz and anorthite. The formation of anhydrite is due to the addition of limestone to prevent flue gas pollution. The quartz-HP (PDF Card: ICDD 01-086-1564) observed in this study is a special quartz that can only be formed under high pressure, thus it is estimated to be derived from the added low-grade limestone. However, no appreciable hump of glass phase was found in the XRD charts, suggesting that glass phases were quite rare in the BA samples due to low incineration temperature less than 1000℃.

Compared to natural sand, BA particles are more fragile and less condensed, and present an irregular shape together with rough surface and porous structure. The surface texture of BA particles changes with particle size. Overall, fine particle is formed by flakes, whereas coarse particle has many pores and is a combination of tiny particles, as shown in **Figs. 3(a)** and **(b)** of SEM images, respectively. The rough surface and porous structure of BA particle would lead to a high liquid-solid ratio and decrease the strength of GP with BA.

2.2 Geopolymer precursors

As discussed latter, when the BA was used as sole precursor, obtained BA-based GP had a small strength. Therefore, the BA was used as fine aggregate to produce GP mortar in the latter experiments. Ground granulated blast furnace slag (BFS) and coal fly ash (CFA) were used together as precursors of GP mortar. The BFS used conformed to Class 4000 of JIS A 6206, and had a density of 2.90 g/cm^3, a specific surface area of 4279 cm^2/g. The used CFA met with JIS II type coal fly ash, having a density of 2.31 g/cm^3, a specific surface area of 4392 cm^2/g, respectively. The chemical compositions of CFA and BFS, analyzed by XRF, are shown in **Tables 3** and **4**. The CaO content of CFA was only 3.61%. These precursors contained very small amounts of heavy metals.

Figures 4 and **5** show the PSD (particle size distribution) curves of BFS and CFA, which were measured by a

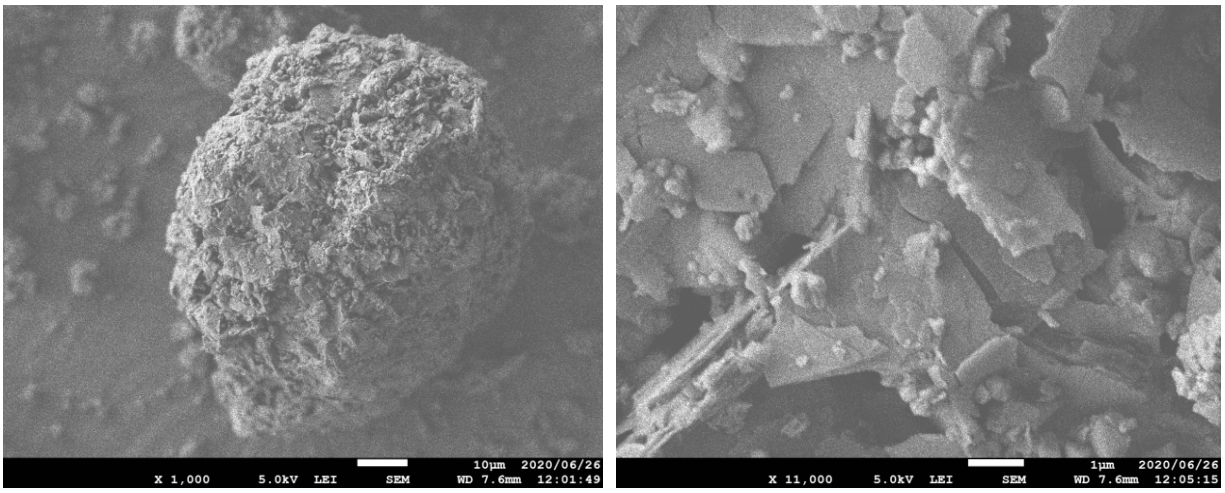

(a) Fine BA particles, 0.075 to 0.15 mm. The magnifications of the images are: Left 1000, Right 11 000.

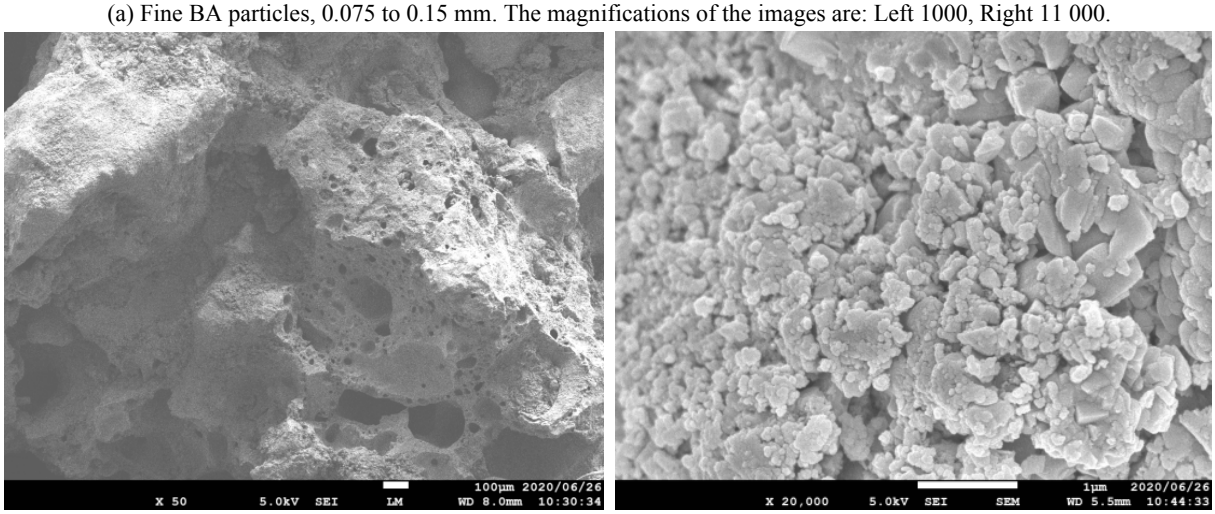

(b) Coarse BA particles, 2.4 to 5.0 mm. The magnifications of the images are: Left 50, Right 20 000.

Fig. 3 SEM images of original BA particles.

Table 3 Chemical compositions of BFS and CFA (mass %).

Precursors	SiO_2	TiO_2	Al_2O_3	Fe_2O_3	MnO	CaO	MgO	Na_2O	K_2O	P_2O_5	SO_3	Cl	Trace elements	Total
BFS	32.68	0.63	13.71	0.37	0.20	45.14	4.92	ND	0.30	0.04	1.80	ND	0.21	100.00
CFA	58.65	1.18	24.66	6.13	0.08	3.61	1.16	1.10	1.62	0.89	0.45	ND	0.47	100.00

[Note] ND: Not detectable.

Table 4 Trace elements of BFS and CFA (ppm).

Precursors	V	Cr	Co	Ni	Cu	Zn	Ga	Ge	Rb	Sr	Y	Zr	Nb	Ba	Pb
BFS	ND	ND	ND	35	ND	ND	ND	ND	ND	600	86	273	ND	736	ND
CFA	400	83	65	149	125	174	68	23	83	1229	ND	410	24	726	123

[Note] ND: Not detectable.

Table 5 SiO_2/Na_2O mole ratios of AA solutions used.

AA solution	WG/NH ratio (by volume)	SiO_2/Na_2O mole ratio
WG	1:0	2.06
AA71	7:1	1.50
AA31	3:1	1.09
AA11	1:1	0.56
NH	0:1	0

laser diffraction type PSD test apparatus. The size of BFS particles was in range of 1.0 to 100 μm, with median of 11.6 μm, but the size of CFA particles was mainly in range of 1.0 to 50 μm with median of 6.7 μm.

2.3 Alkali-activator solution

In this study, an aqueous solution of JIS K 1408 Type 1 sodium silicate diluted with water at a volume ratio of 1: 1 (hereinafter referred to as WG), and a caustic soda aqueous solution having a molar concentration of 10 M (hereinafter referred to as NH) were used as alkali-activator (AA) solution. Usually, 8 to 14 molar NaOH solutions are used to prepare AA solution of other GPs. For balancing the cost and activation capacity of AA, 10 molar NaOH solution was employed in this study. We also used mixtures of WG and NH in volume ratios of 7:1, 3:1, 1:1, abbreviated as AA71, AA31, and AA11, respectively, as AA solution for discussing the effect of NH content or alkalinity of AA solution on the properties of GP. **Table 5** shows the mole ratio of SiO_2 and Na_2O in the 5 kinds of AA solution.

Table 6 Mixtures of BA-based GP.

Series	Type of AA	BA	AA/BA
BA-WG	WG	2/'20	0.35
BA-71	AA71		
BA-31	AA31		
BA-NH	NH		

2.4 Fabrication and curing of specimens

In order to confirm the reactivity of BA in AA solution, the specimens for the strength tests were first produced by using the GP mixtures of BA and AA solution (denoted as BA-based GP), i.e., the BA was used as GP precursor. The mix proportions of BA-based GPs are shown in **Table 6**. The BA sample discharged in Feb. 2020 was used, and the AA solutions contained different amounts of WG aqueous solution from zero to 100% by volume. The liquid-solid ratio of AA solution to BA was 0.35 by mass.

The BA-based GPs were mixed by a mortar mixer with planetary motion blade in our laboratory with 20±3ºC and RH 60±10%. However, if the mixing time was less than 10 minutes, the GPs could not be evenly mixed. This is because BA is not a powder, but consists of porous, highly absorbent particles with few fine particles. Some of the BA particles absorbed the AA solution, which initially contacted with the added AA solution. This made it difficult to mix evenly the AA solution and all the BA particles in a short mixing time. With the increase of mixing time, the blade of mixer broke some BA particles, so that the amount of fine powder was increased, resulting in the GP becoming fine-grained and

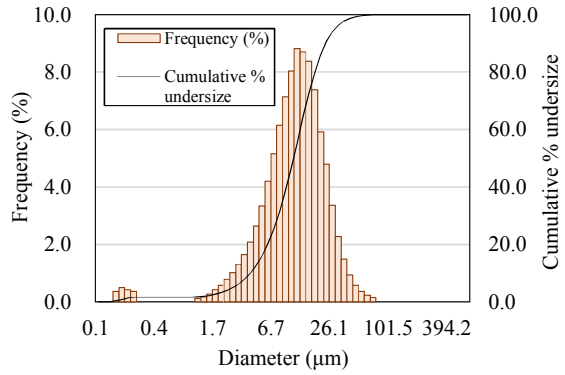

Fig. 4 Particle size distribution of BFS.

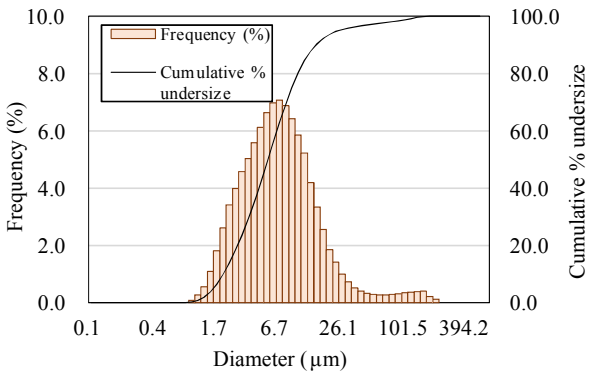

Fig. 5 Particle size distribution of CFA.

Table 7 Mixtures and curing methods of BFS/CFA-based GP mortars using BA as fine aggregate.

Series	Curing method	Type of AA	BA sample	AA/P	BFS/P	CFA/P	BA/P
23- 40 -WG	H	WG	23/'19	0.6	0.4	0.6	1.5
6- 40 -WG			6/'19				
8- 40 -WG			8/'19				
10- 40 -WG	A, H		10/'19				
12- 40 -WG	H		12/'19				
10- 70 -WG	A, H		10/'19		0.7	0.3	
10-100-WG					1.0	0.0	
10- 40 -NH	H	NH			0.4	0.6	
10- 40 -11		AA11					
5- 40 -WG	A, H	WG	5/'20				
5- 70 -WG	A				0.7	0.3	

[Notes] 1) H: heat-curing, A: ambient curing, P: precursors.
2) The ratios of raw materials are by mass.

uniform. Therefore, strictly speaking, the BA-based GPs were GP mortar systems with tiny BA particles as precursor, and coarse BA particles that were not broken by the mixing as fine aggregate. We also found that the required mixing time became long as WG content in the AA solutions increased. This is because that the WG solution has a higher viscosity than the NH solution. In order to ensure the same experimental conditions and to facilitate the comparison of experimental results, the mixing times for all the BA-based GPs were fixed at 10 minutes.

After mixing, each BA-based GP sample was filled into a 3-cell steel mold and vibrated by a table vibrator. The specimens for strength measurement were prismatic in size of 4×4×16 cm, which were first cured in the 80ºC air for 24 hours, followed by curing in the 20ºC air. Here, this curing method is briefly called heat-curing. The BA-based GP specimens were sealed with plastic wrap during the entire curing period for preventing rapid drying. In case of the heat-curing, if demolding is late, the specimen may bond with the steel mold, which causes surface damage to the specimen. Hence, demolding was performed 3 hours after the beginning of heat-curing. After demolding, the specimens were resealed and placed back into the 80ºC chamber and continued to be cured for 21 hours.

On the other hand, in the BFS/CFA-based geopolymer mortars, the BAs were used as fine aggregate, BFS and CFA were used as precursors (P). The used BA samples, mix proportions and curing methods of BFS/CFA-based GP mortars are shown in **Table 7**. The ratio (BA/P) was fixed to be 1.5 by mass. If the BA/P ratio was higher than this value, a large amount of AA solution was required due to the high absorption of BA. The AA/P ratio was 0.60 by mass, below which mixing the GP mortars with the BA/P of 1.5 became very difficult. The BFS content was adjusted from 40% to 100% to investigate its effect on the properties of BFS/CFA-based GP mortars.

The mixing of GP mortars used the same mixer mentioned above. Followed by mixing BA, BFS and CFA for about 120 seconds until they became even, the AA solution was added and further mixed for 150 seconds. Immediately after mixing, each GP mortar sample was filled into molds and vibrated with a table vibrator to produce test specimens. Two types of specimens were prepared, which were prismatic specimen with dimensions of 4×4×16 cm, and cylindrical specimen with diameter of 10 cm and height of 20 cm. The former was used for strength tests, but the latter was employed in the accelerated carbonation test.

Curing of GP mortar specimens was carried out in two ways: heat-curing, as described above, and ambient curing. Ambient curing was an air curing in a 20°C chamber, during which the specimens were sealed with plastic wrap. Demolding was performed at 24 hours age in case of ambient curing.

2.5 Test methods of properties

2.5.1 Setting time test

The final setting times of BFS/CFA-based GP mortars were measured with a Vicat needle apparatus, following JIS R 5201 (Physical Testing Methods for Cement). Originally, JIS R 5201 is specified for cement paste. Since the amount of bottom ash used in the GP mortars was smaller (BA/P=1.5), compared to general mortar using natural sand, it is considered that the effect of BA particles on the measurement result of setting time was small. By using the same measurement method, the discussion could be carried out without any lack of reliability. Right after GP mortar was mixed, the test was conducted.

2.5.2 Strength test

At the curing age of 7 days in case of BA-based GP, or 28 days in case of BFS/CFA-based GP mortar, three-points bending test was first performed for each group of prismatic specimens with dimensions of 4×4×16 cm, using an Amsler universal testing machine. Next, compressive strength was measured, using the fractured pieces of the bending test. The flexural and compressive loads were applied on the sides perpendicular to the casting direction of prismatic specimen. The flexural strength was an average of three prismatic test specimens, but the compressive strength was an average of six fractured pieces.

Table 8 Detection limits of 8 tracedheavy metal elements (mg/L).

Element	As	Cd	Cr	Cu	Mn	Pb	Se	Zn
Detection limits	0.020	0.003	0.004	0.013	0.004	0.021	0.053	0.011

[Note] Cr is the total amount of Cr (III) and Cr (VI).

2.5.3 Accelerated carbonation test

The accelerated carbonation test was performed for the BFS/CFA-based GP mortars, using two cylindrical specimens with diameter of 10 cm and height of 20 cm for each series, in accordance with JIS A 1153 (Method of Accelerated Carbonation Test for Concrete). After 28 days curing, both end surfaces of every cylindrical specimen were sealed with aluminum foil tape to ensure that CO_2 diffuses into the specimen only through the circumferential surfaces. Then, the specimens were placed into an accelerated carbonation test chamber with 5±0.2% of CO_2 concentration, 20±2°C, and RH 60±5%. At an interval of one week, the mortar specimen was cut at 35-40 mm intervals to measure the carbonation depth. It should be noted that during the cutting, in order to ensure that the alkali matters were not washed away, sprinkling water was not used as dust prevention. The carbonation depth was measured within 5 minutes after spraying phenolphthalein 1% ethyl alcohol solution on the freshly cutting surface. After sealing the cutting surface with the aluminum foil tape, and the remaining portion of the specimen was returned to the chamber. The carbonation depth of each specimen was an average of 8 measurement points distributing equally on the circumference of the cutting surface. The accelerated carbonation test lasted 8 weeks.

2.5.4 XRD and SEM/EDS analyses

The BA-based GPs and the BFS/CFA-based GP mortars were analyzed by XRD. After the compressive strength test, the broken specimen was crushed to prepare XRD sample. The XRD analysis was under the conditions: 40 kV and 30 mA of X-ray power, 2 degrees/min. of scanning speed and 3.0 to 60 degrees (2θ) of scanning angle range at 0.02 degree steps. The BFS, CFA and BA used were also analyzed under the same conditions.

Two types of geopolymers were observed by SEM, and the EDS (Energy Dispersive X-ray Spectroscopy) analysis was also conducted in order to evaluate the microstructure and the reaction products of the geopolymers using the BA. The SEM/EDS analysis samples were additionally prepared by mixing geopolymers. Dried samples were impregnated by embedding with epoxy resin, then they were polished flat after hardening at room temperature. Based on the results (mole percentage ratios of elements) of EDS analysis at the selected spots, the molar percentage of each oxide was calculated, and then the ratio (C+M)/(N+K) of the sum of the molar percentages of CaO and MgO to the sum of the molar percentages of Na_2O and K_2O was further calculated for evaluating the chemical components at the selected spots.

2.5.5 Leaching test of heavy metal

To evaluate the potential leaching of heavy metals from original BA and the GP mortar with addition of the BA as fine aggregate, leaching tests were conducted. After the compressive strength test of GP mortars, the fractured specimens were crushed and then sieved out 0.6 to 4.75 mm particles. 2.0 g sample was taken to put into a polypropylene beaker filled with 40 ml leachate and the beaker was further sealed with plastic wrap. Three kinds of leachate used were phthalate pH standard solution (pH 4.01), neutral phosphate pH standard solution (pH 6.86), and deionized water (pH 7.0 in theory), respectively. The beaker was placed in an ultrasonic device with deionized water and oscillated with 28 kHz ultrasonic waves for 10 minutes at ambient temperature (about 20ºC). Then, the solutions were filtered to get the extraction liquid with the filter paper that had the maximum opening size of 15 μm, meeting with JIS P3801, Class 3.

This preparation method of extraction liquid was referred to the rapid analysis method (ultrasonic pretreatment) specified by the Bureau of Environment, Tokyo Metropolitan Government in 2009 (TMEB 2009), here called ultrasonic oscillation method, in which the solid-deionized water ratio is 1:10 (kg/L). However, in case of alkaline solid sample, the solution with 1:10 of solid concentration easily changes to be alkaline. Therefore, in this study, the solid-leachate ratio was set to be 1:20 (kg/L), and the standard acidic and neutral buffers mentioned above were used as leachates to reduce the pH fluctuation. When deionized water was used as leachate, it actually changed to be alkaline (pH was unknown, but should be over 7.0) during the leaching process of alkaline GP sample, which was equivalent to alkaline leachate.

Eight kinds of heavy metal elements were traced, including chromium (Cr), manganese (Mn), copper (Cu), lead (Pb), zinc (Zn), arsenic (As), selenium (Se), and cadmium (Cd). The leaching concentration (Ci) of each metal element in the extraction liquid was determined by ICP-AES (induction coupled plasma atomic emission spectrometry) analysis. **Table 8** shows the detection limits for the 8 kinds of trace metal elements.

In this study, we have tried to calculate the immobilization efficiency (IE) of heavy metal elements. The masses of raw materials used in 2 g of GP mortar sample were calculated based on the mix proportions of the GP mortar, and then the maximum leaching concentration (Cm) of the GP mortar was calculated for each trace element, according to the chemical compositions of the raw materials measured by XRF, and assuming that the trace elements were not immobilized at all. The IE of trace element was defined as (Cm-Ci)/Cm×100%. When calculating the Cm, the trace metal elements in the AA

solution were ignored due to extremely small quantities, but the trace elements in the BFS and the CFA were taken into account based on the XRF results shown in **Table 4**. The used GP mortar samples were not dried before the leaching test so that moisture content was unknown. Therefore, we had to use two element amounts to calculate the Cm respectively. One was calculated on the assumption that the sample before leaching test was absolutely dry. Thus, this element amount was slightly larger than the value given by the mix proportions shown in **Table 7**. In addition, another element amount was calculated based on the mix proportions, assuming that the GP mortar sample had no moisture evaporation. For this reason, the IEs with and without complete moisture evaporation were calculated, respectively. The actual IE should lie between the upper and the lower IE values. However, the IE difference between the upper and the lower IE values was less than 0.5% for the metal elements. Therefore, the median of the upper and the lower IE values was used to evaluate the immobilization ability of GP mortar.

In addition, the extraction liquids of series 10-40-WG-H and series 10-40-NH were prepared according to the recycled construction material evaluation method (JSCE 2003), in order to determine whether the leaching concentrations of trace heavy metals meet the environmental limits of recycled construction materials specified by Japan Institute of Country-Ology and Engineering with reference to the environmental standards for soil contamination. The samples of two series of GP mortars were cured by the heat-curing method and stored in the ambient air for 1 year. This method specifies that leachate should have a pH of about 4.0, the leaching solution that contains solid sample with a size of 20 to 50 mm and leachate by a liquid-solid ratio of 10 mg/L should be stirred for 24 hours, and the extraction liquid is collected by filtering the solution by a filter paper with the opening size of 0.45 μm. Hereafter, this method is briefly called stirring method.

The leachate, used in the stirring method, was a phthalate buffer solution with a pH of 4.01. First, dried GP mortar was crushed, and one grain with a size of about 20 mm was selected and placed in a plastic container having diameter of about 75 mm and height of about 40 mm. Then, the leachate was added until the liquid-solid ratio reached to 10 mL/g, and a rotor was put into the container for magnetic stirring. The magnetic stirring was performed for 24 hours at a speed of about 200 rpm. After the stirring, the leaching solution was filtered firstly through a qualitative filter paper with a maximum opening size of 10-15 μm, and then through a membrane filter with a maximum opening size of 0.45 μm to collect extraction liquid. The collected extraction liquids were also analyzed by the ICP-AES.

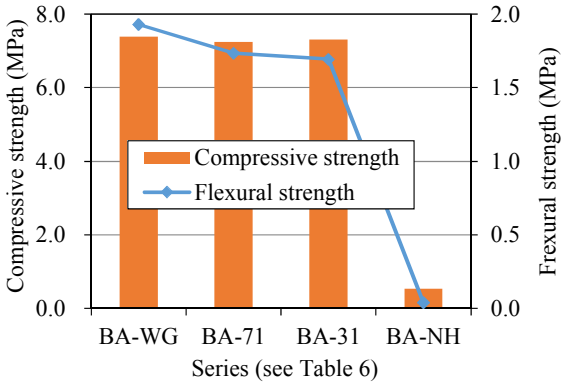

Fig. 6 Strengths of BA-based GP.

3. BA-based geopolymer using BA as precursor

3.1 Flexural and compressive strengths

Figure 6 shows the strength test results of BA-based GPs at 7 days age, which were cured by the heat-curing method. When the used AA solution was only sodium hydroxide solution, flexural and compressive strengths were very small. However, when WG, AA71, and AA31 were used as AA solutions, BA-based GPs had almost the same compressive strength (7.3 MPa), but the flexural strength slightly decreased with the increase of NH content in the AA solutions. This suggests that Si^{4+} and Al^{3+}, which are necessary ions for the formation of N-A-S-H gels and C-A-S-H gels, are less leached by the NH solution. This is because BA has less amorphous phases, according to the XRD results explained in the latter. However, the presence of free Ca^{2+} in BA or easy dissolution of Ca^{2+} in alkaline solution contributes to the strength development of GP using WG solution as a part or the whole of the AA solutions. Zhu *et al.* (2016) reported that the geopolymer with a liquid-solid ratio of 1.0 had small density of 1.0 g/cm^3 and low compressive strength of 2.8 MPa, which used ground BA (<150 μm) as sole precursor and was cured at 80ºC for 3 days. The porous structure of BA resulted in the necessity of large liquid-solid ratio. Moreover, grinding BA requires energy. Therefore, using ground BA as precursor to synthesize high performance geopolymer is not practical, though BA has somewhat reactivity in the NH solution.

3.2 Chemical and micro-structure analysis

3.2.1 XRD analysis

Figure 7 shows the XRD patterns of three series of BA-based GPs using the 2/'20 BA sample. It was found that regardless of the AA solutions used, three BA-based GPs had the same crystalline phases, which were also found in the original BA except gobbinsite, although the original BA and the GP had different peak intensity for the same crystalline phase. However, the C4 (hydrotalcite, $Ca_4Al_2O_6Cl_2{\cdot}10H_2O$) of BA was lost in the GPs. We believe that the C4 of BA was dissolved by the AA solutions, and the Na^+ in the AA solutions allowed a further conversion of C4 to gobbinsite in the GPs. Moreover, from the XRD patterns, a low hump was observed in the range of 25 to 35 degrees (2θ). This suggests that a small amount of amorphous gels was formed in the GPs. It was

found that all the particle size fractions of BA contain SiO_2 and Al_2O_3 amorphous phases, through the leaching test of BA in NaOH solution and the ICP-AES analysis (Maldonado-Alameda *et al.* 2020). As discussed above, though series BA-NH using NH as AA solution had a very small strength, this result suggested that there was active phase in the BA. Original amorphous SiO_2, Al_2O_3 and the dissolution of C4 contributed to the polymerization reaction of BA-based GP.

3.2.2 SEM analysis

Figure 8 shows the SEM images of two series of BA-based GPs, in which the used BA was discharged in Feb. 2020, and the AA solutions were the WG solution, and the AA31 solution, respectively. As shown in the SEM images (1) and (4) of **Fig. 8**, the GP using sole WG as AA solution was relatively denser than the GP using the AA31 solution, and there were more cracks in the latter. Long time mixing of GP crushed part of BA par-

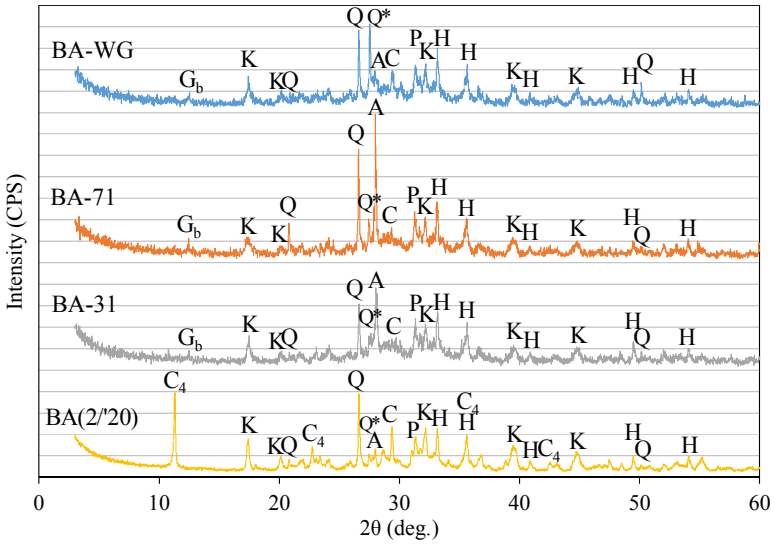

[Notes] Q: Quartz, SiO_2; Q*: Quartz-HP, SiO_2; C: Calcite, $CaCO_3$; A: Anorthite, $CaAl_2Si_2O_8$; K: Katoite, $Ca_3Al_2(OH)_{12}$; H: Hematite, Fe_2O_3; P: Anhydrite, $CaSO_4$; C_4: Hydrotalcite, $Ca_4Al2O_6Cl2{\cdot}10H_2O$; G_b: Gobbinsite, $Na_4Ca(Si_{10}Al_6)O_{32}{\cdot}12H_2O$.

Fig. 7 XRD patterns of BA-based GPs.

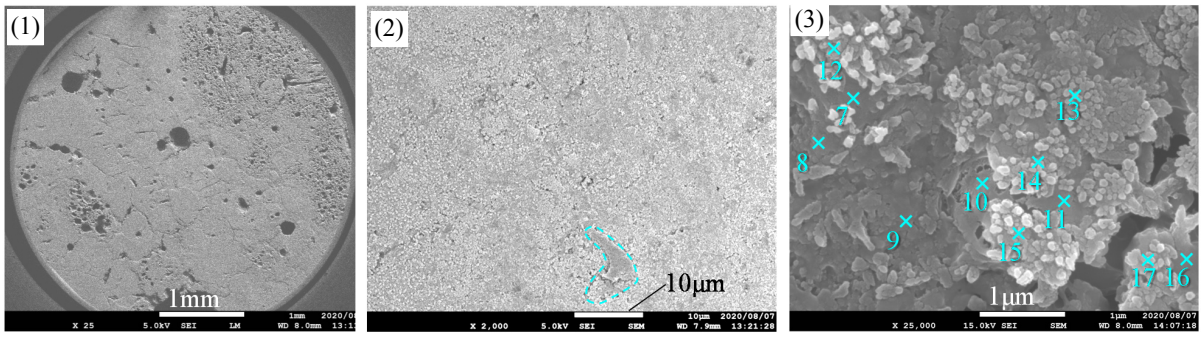

(a) BA-based geopolymer using WG solution, series BA-WG. The magnifications of the images are: (1) 25, (2) 2000 and (3) 25 000.

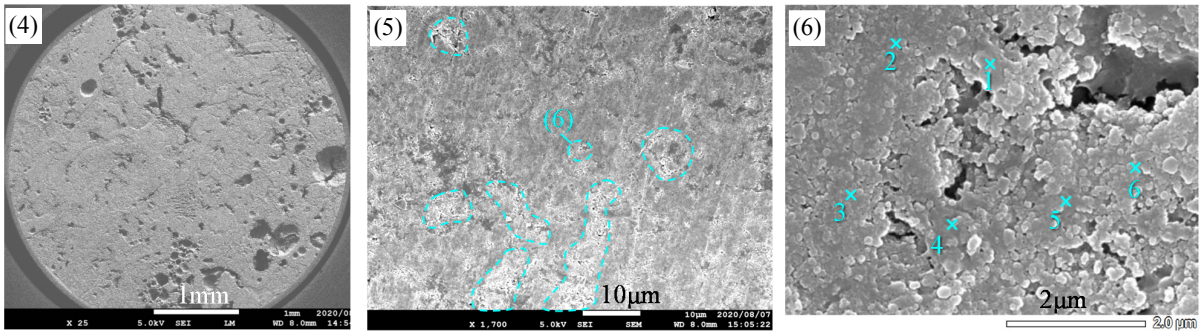

(b) BA-based geopolymer using the AA31 solution, series BA-31. The magnifications of the images are: (4) 25, (5) 1700 and (6) 20 000.

Fig. 8 SEM images of BA-based geopolymers.

Table 9 Results of SEM/EDS point-analysis for two BA-based geopolymers.

Spot	Mole percentage of oxide and chloride (%)									(C+M)/(N+K)*	(Al+Si)/(Na+K+Ca)**	Compound
	SiO_2	TiO_2	Al_2O_3	CaO	MgO	Na_2O	K_2O	SO_3	Cl			
1	60.01	4.18	10.25	4.32	8.44	9.26	2.02	0.00	1.51	1.13	3.07	Gobbinsite
2	60.57	3.95	9.80	3.59	9.89	9.08	1.89	0.00	1.24	1.23	3.14	Gobbinsite
3	62.62	2.75	11.94	4.04	5.82	9.97	1.89	0.00	0.97	0.83	3.07	Gobbinsite
4	60.48	2.87	11.70	4.34	7.08	10.23	1.89	0.00	1.40	0.94	2.93	Gobbinsite
5	61.13	3.80	11.01	3.80	7.81	9.17	2.03	0.00	1.25	1.04	3.21	Gobbinsite
6	60.03	3.46	11.21	3.53	8.05	10.75	1.90	0.00	1.06	0.92	2.71	Gobbinsite
7	58.61	0.00	10.64	20.99	0.93	6.65	1.35	0.00	0.83	2.74	2.31	C-A-S-H
8	59.91	0.00	10.17	16.90	1.00	8.79	1.22	1.19	0.81	1.79	2.30	C-A-S-H
9	61.24	0.00	7.05	19.88	1.24	8.64	0.94	0.00	1.00	2.20	1.95	C-A-S-H
10	44.48	0.00	14.11	35.00	0.00	5.81	0.60	0.00	0.00	5.46	1.55	C-A-S-H
11	47.81	0.00	13.67	29.24	0.00	6.00	0.78	1.86	0.64	4.31	1.85	C-A-S-H
12	46.07	0.00	12.16	31.05	1.01	6.19	0.88	1.70	0.94	4.53	1.63	C-A-S-H
13	54.96	0.00	5.22	26.51	1.82	8.19	0.70	1.76	0.85	3.19	1.54	C-A-S-H
14	43.21	0.00	12.16	34.30	1.26	5.96	0.60	1.88	0.63	5.42	1.44	C-A-S-H
15	46.63	0.00	15.58	31.01	0.00	6.05	0.72	0.00	0.00	4.58	1.81	C-A-S-H
16	57.92	0.00	11.62	21.06	1.09	5.83	0.78	1.09	0.61	3.35	2.50	C-A-S-H
17	62.28	0.00	13.19	14.69	0.86	5.98	0.86	1.66	0.47	2.27	3.36	Gobbinsite

[Notes] *: Obtained from the molar percentages of metal oxides.
**: Obtained from the molar percentages of metal elements.

ticles, but large BA particles were still found in the GPs, which had more pores in them. The voids in GP matrix were air bubbles involved during the mixing. From the SEM images (2) and (5) of **Fig**. **8**, it was found that series BA-WG showed sponge-like structure, while in series BA-31, there were dense regions along with the sponge-like regions. As explained latter, the dense regions were composed of N-A-S-H gels, and the sponge-like region was formed by C-A-S-H gels. The high alkalinity of the AA31 solution containing sodium hydroxide (NaOH) might promote the leaching of Al^{3+} from the BA, allowing the formation of N-A-S-H gels. We also found that there were numerous crystal particles in the two BA-based GPs as shown in images (3) and (6) of **Fig**. **8**. For clearing up their compositions, EDS analysis was performed. The results of EDS point analysis are shown in **Table 9**.

From **Table 9**, the particles in series BA-WG had the compositions of C-A-S-H, but the particles present in series BA-31 had the compositions of N-A-S-H. In some cases, e.g., heat-curing, N-A-S-H gel, possibly C-A-S-H gel would be crystallized to change zeolite surrounded by N-A-S-H gels or C-A-S-H gels (Palomo *et al.* 2004; Feng *et al.* 2005; JCI 2017). There are many types of zeolite in zeolite mineral family, including gobbinsite. The gobbinsite has two types: $Na_4Ca(Si_{10}Al_6)O_{32}{\cdot}12H_2O$ and $Na_4(Ca, Mg, K_2)Al_6Si_{10}O_{32}{\cdot}12H_2O$. The (Si+Al)/(Na+Ca+K) ratio, being an element mole ratio, is 3.2 for the former, and 2.3 for the latter. Hence, we considered that in spots 1 to 6 of series BA-31, there were blended minerals of two types of gobbinsite, i.e., crystallized N-A-S-H gels, and spot 17 of series BA-WG contained gobbinsite minerals too, i.e., crystallized C-A-S-H gels. Spots 7, 8, 16 had a (Si+Al)/(Na+Ca+K) ratio of around 2.3 or 2.50, but it was judged there were C-A-S-H gels at these spots because no crystallization morphologies were observed. In other places of series BA-31, C-A-S-H gels, metallic aluminum (Al), and anorthite crystal were also detected by the EDS point analysis (SEM images were omitted here). Al and anorthite came originally from the BA. It is noted that gobbinsite and anorthite were also found in the XRD analysis, as mentioned above.

4. BFS/CFA-based geopolymer mortar using BA as fine aggregate

4.1 Setting time

Figure 9 shows the test results of final setting times of the BFS/CFA-based GP mortars using BA as a fine aggregate. First, for the same BA sample (10/'19), the larger the BFS content, the shorter the setting time of GP mortar, which is consistent with BFS/CFA-based GP using natural sand. However, the difference in final setting times was only about 20 minutes between 40% and 100% BFS content. That is to say, decreasing BFS content in precursors cannot largely prolong the setting time of BFS/CFA-based GP. Recently, a retarding technology has been developed by pre-heating BFS at 700℃ (Li *et al.* 2019).

Next, it was found that for the same BFS content (40%), the final setting time of BFS/CFA-based GP mortars depended on the discharge time of BA. When 23/'19 and 12/'19 BA samples were used, the setting time was as short as 65 minutes. However, the GP mortar, using any of the 6/'19, 8/'19, and 10/'19 BA samples, had a relatively long final setting time, being 120, 110, and 130 minutes, respectively. This indicates that the BA discharged in warm season leads to a long setting time of GP.

As discussed in Section 3.2.1, the C4 crystal mineral, which is hydrotalcite, disappeared in GP and might produce gobbinsite and GP gels. The 23/'19 and 12/'19

BA samples had a higher content (larger peak intensity) of C4 than other BA samples, as shown in **Fig. 2**. Though the XRD analysis was not quantitative because no standard matter was added, from the height of peak, the comparison of crystal contents may be possible as a reference. This is one of reasons why the GP mortar using 23/'19 and 12/'19 BA samples had a shorter setting time. Then, Ca^{2+} leaching from the C4 mineral may react rapidly with sodium silicate. Among the 6/'19, 8/'19, and 10/'19 BA samples, the 8/'19 BA sample had most fine particles and the 10/'19 BA sample had the lowest peak of C4. These features may explain the difference in the final setting time between the three GP mortars (series 6-40-WG, 8-40-WG, and 10-40-WG), using 6/'19, 8/'19, and 10/'19 BA samples, respectively.

In addition, when AA11 and NH were used as AA solutions, respectively, the final setting time was significantly reduced, compared to when WG solution was used. This was probably because the polymerization reaction of the precursors was activated due to the increase in alkalinity of the AA solution containing NH. Since Si^{4+} coming from WG solution promoted the polymerization reaction, the setting time of series 10-40-11 was little shorter than that of series 10-40-NH.

4.2 Flexural and compressive strengths

The strengths of the GP mortars are shown in **Fig**. **10**. First, as usual GP mortar using natural fine aggregate, the larger the BFS content in precursors, the larger the strength of GP mortar using BA, and the heat-curing yielded a higher strength than the ambient curing. From **Fig**. **10**, it was also found that for the same BFS content (40%) and curing method, the strengths of GP mortars changed with the discharge time of BA, series 8-40-WG, 10-40-WG, and 12-40-WG had larger strengths than other series using 40% BFS and WG solution, and the strengths of two series of 10-40-WG (WG-H and WG-A) using 10/'19 BA sample were higher. It is considered that the strength of GP mortar partly depends on the strength of fine aggregate used. The 8/'19 and 10/'19 BA samples had larger densities, suggesting they were denser and stronger than other BA samples. The 12/'19 BA sample with fineness modulus of 3.30 was the coarsest among the five kinds of BA samples, though its density was not large. As described in Section 2.1, fine BA particles were composed of flakes, but coarse BA particles contained many small particles. Compared to flake assembly, particle assembly is strong. Thus, series 12-40-WG had a relatively high strength. The setting time of GP mortar using BA was greatly affected by the chemical compositions of BA, but the strength was more affected by BA's physical properties rather than its chemical compositions.

When NH was added in AA solution, the strength of GP mortars significantly decreased, as compared with the GP mortar using only WG. Li (2016b) reported that metallic aluminum (Al) contained in the melting slag of incineration ash causes foaming and expansion of GP adding NH solution, because of the formation reaction of hydrogen gas [$2Al+6H_2O \rightarrow 2Al(HO)_3+3H_2\uparrow$]. Similarly, BA should contain the Al that originally comes from the aluminum foil in solid wastes. The foaming reaction of Al may be one of the reasons for the decrease in strength of GP using NH solution as part or all of the AA solution. Another reason was the discontinuous structure of GP mortar using only NH solution, containing many granulated C-A-S-H and N-A-S-H, as discussed later in Section 4.5.2. The less continuous C-A-S-H gels and N-A-S-H gels are thought to be due to the lack of Si^{4+}, which can be provided by the WG solution besides precursors. It should be noted that though the BA has porous structure, the GP mortars using sole WG solution had high compressive strength up to 50 MPa, even if only 40% BFS was used. The alkalinity (pH>12.0) and the dissoluble

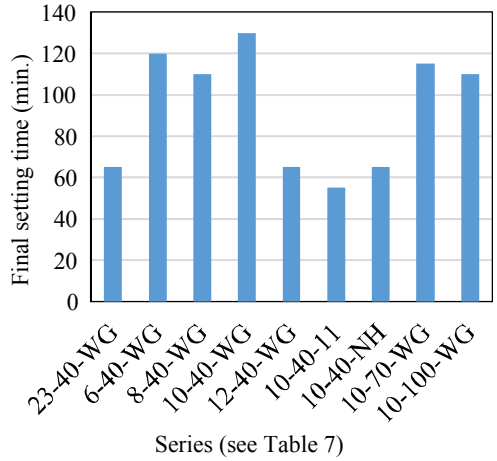

[Note] Series name: Discharge month of BA - Mixing ratio (% of BFS - Type of AA.

Fig. 9 Final setting times of GP mortars using BA as fine aggregate.

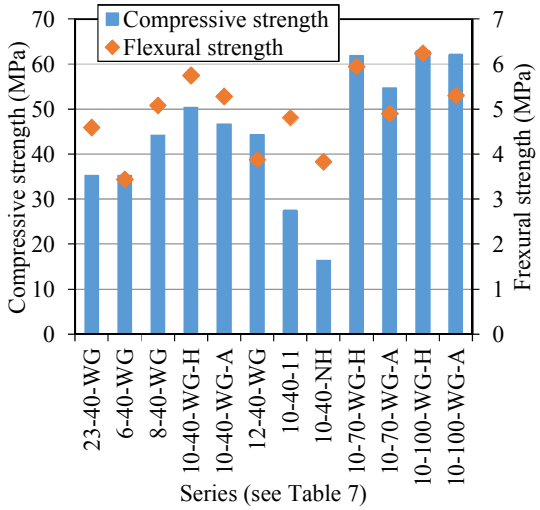

[Note] Series name: Discharge month of BA - Mixing ratio (%) of BFS – Type of AA - Curing method (H and No labeling: heat-curing, A: ambient cuing).

Fig. 10 Strengths of BFS/CFA-based GP mortars using BA as fine aggregate.

Table 10 Carbonation rate coefficients of BFS/CFA-based GP mortars with BA.

Series	Regression line	Coefficient of determination (R^2)	Carbonation rate coefficient
5-70-WG	y = 3.397x-2.375	0.966	3.397
5-40-WG-A	y = 5.037x-3.777	0.963	5.037
5-40-WG-H	y = 3.151x-1.652	0.963	3.151

[Notes] 1) y is the carbonation depth (mm).
2) x is the square root value of days of accelerated carbonation.

calcium of BA may contribute to the high strength of GP with BA. The former promotes the dissolution of precursors, while the latter can react with WG. Further investigation is necessary. The absence of sodium hydroxide will certainly be beneficial in reducing cost and efflorescence of geopolymer. Some of Na^+ from the AA solution is weakly associated with water molecules as $Na(H_2O)^{n+}$, and thus easily leach out to form Na_2CO_3 on the GP surface, so-called efflorescence (Zhang *et al.* 2015). Therefore, excessive alkali content tends to cause efflorescence.

4.3 Carbonation resistance

Figure 11 shows the coloration of series 5-70-WG after spraying phenolphthalein 1% alcohol solution on the cutting surface of the GP mortar specimen that was subjected to 4 weeks of the accelerated carbonation. In the non-carbonated area, many BA particles were purple, implying that BA is alkaline.

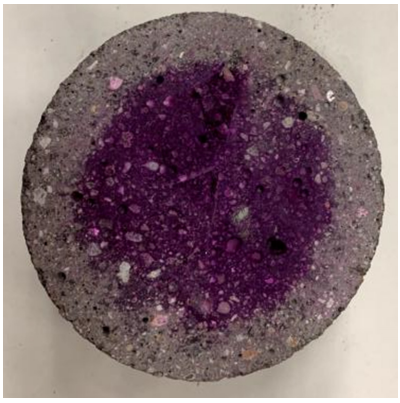

Fig. 11 Coloration of carbonated BFS/CFA-based GP mortars using BA, Series 5-70-WG.

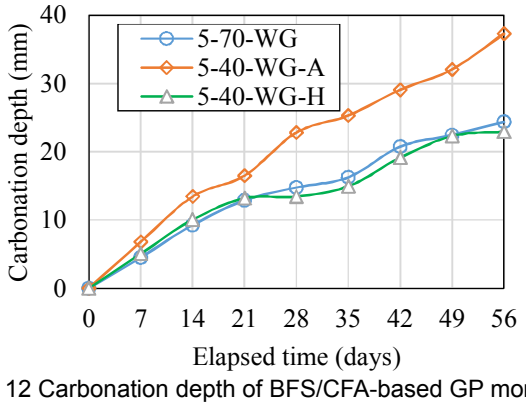

Fig. 12 Carbonation depth of BFS/CFA-based GP mortars using BA.

Figure 12 shows the relationship between the carbonation depth and the accelerated carbonation period for the BFS/CFA-based GP mortars with BA as fine aggregate. It was found that the lower the BFS content, the lower the carbonation resistance of GP mortar, and the heat-curing yielded higher carbonation resistance for the same GP mortar mixture. These results are consistent with BFS/CFA-based GP mortar and concrete with natural sand (Li and Li 2018). By a regression analysis on basis of assuming that the carbonation depth is a square root function of carbonation time like as Portland cement concrete, we got the carbonation rate coefficients for the three GP mortars, as shown in **Table 10**. Compared to the BFS/CFA-based GP mortar using natural sand (Li and Li 2018), the use of BA resulted in a low carbonation resistance. The porous structure of BA particle may have an adverse effect on the carbonation resistance of GP materials. Smaller BA/P may be another reason. In normal mortars, sand content is generally more than twice that of the binder, the sand, which is denser than the binder matrix, hinders the diffusion of CO_2.

It is generally recognized that BFS/CFA-based GP materials have a lower carbonation resistance than Portland cementitious materials, and the GP using only WG as AA solution generally has lower carbonation resistance, compared to the GP using a mixed solution of WG and NH (Li and Li 2018). Arbi (2016) also reported that more intense and deeper carbonation was found in geopolymer than in Portland cement mortars. However, Bernal *et al.* (2013) argued that the accelerated carbonation test at high CO_2 concentrations is likely to provide unrepresentative or misleading results with natural exposure of BFS/CFA-based GP. How to evaluate and improve the carbonation or neutralization resistance of GP materials is an important issue waiting to be solved for the practical application of GP binder in reinforced concrete (Li *et al.* 2020). That is, even if the use of BA instead of natural sand leads to a low carbonation resistance of GP, this is not a new problem resulted from the use of BA.

4.4 Leaching of heavy metals

Table 11 shows the leaching concentrations of heavy metal elements (HME) from the precursors and the BA samples discharged in different months. The lower the pH of leachate, the larger the leaching concentration regardless of trace elements. Compared to BFS, the used CFA contained more HMEs. From the BA samples, the leaching concentrations of Cr, Cu, Mn, and Zn were relatively large, but only in acidic leachate, the leaching

Table 11 Leaching concentration (mg/L) of trace heavy metal elements from raw materials.

Element	pH of leachate	BFS	CFA	23/'19 BA	6/'19 BA	8/'19 BA	10/'19 BA	12/'19 BA
Cr*	4.01	0.03	0.15	0.13	0.11	0.09	0.16	0.12
	6.86	0.03	0.10	0.13	0.09	0.07	0.07	0.09
	Water	ND	0.05	0.07	0.06	0.04	0.04	0.05
Cu	4.01	ND	0.14	0.03	0.31	0.37	1.60	ND
	6.86	ND	0.01	0.01	ND	0.01	0.01	0.01
	Water	ND	ND	ND	ND	0.01	0.01	0.01
Mn	4.01	2.44	0.66	0.09	0.28	0.40	0.34	ND
	6.86	0.09	0.07	0.01	0.01	0.01	0.01	ND
	Water	ND	ND	ND	ND	ND	ND	ND
Pb	4.01	ND	ND	ND	0.03	0.01	0.07	ND
	6.86	ND	ND	ND	ND	ND	ND	ND
	Water	ND	ND	ND	ND	ND	ND	ND
Zn	4.01	0.02	0.13	0.12	2.39	3.49	7.46	ND
	6.86	ND	0.01	ND	ND	0.02	0.01	ND
	Water	ND	ND	ND	0.01	0.01	0.02	0.02
As	4.01	0.03	0.23	0.03	0.03	0.03	0.03	0.02
	6.86	0.01	0.12	0.02	0.01	0.01	0.01	0.01
	Water	0.01	0.01	0.01	0.01	0.01	0.01	ND
Cd	4.01	ND	ND	ND	ND	0.02	0.01	ND
	6.86	ND	ND	ND	ND	ND	ND	ND
	Water	ND	ND	ND	ND	ND	ND	ND
Se	4.01	ND	ND	ND	ND	ND	ND	ND
	6.86	ND	ND	ND	ND	ND	ND	ND
	Water	ND	ND	ND	ND	ND	ND	ND

[Notes] 1) ND: Not detectable due to exceeding the limit of ICP-AES device.
2) Cr* is total amount of Cr (III) and Cr (VI).

of Pb and Cd were detected for part of BA samples, and the Se leaching was not detected for all the BA samples and all the kinds of leachates used. That is to say, these BA samples contained low levels of Pb, Cd and Se. In addition, no consistent correlation was found between leaching concentrations of HMEs and BA's discharge time.

Table 12 shows the leaching concentrations of HMEs from the GP mortars in different leachates, measured by the ultrasonic oscillation method. In any kind of the leachates, the leaching of Cd and Se was too low to be detected at this time due to the small contents in the BA samples, meeting the two leaching limits (see **Table 13**) for two types of recycled construction materials of general waste incineration residue (JSCE 2003), which are used in contact with water, and without direct contact with water, respectively. The content of Se in raw materials was so few that it could not be detected in the XRF analysis. Moreover, Se peaks in ICP-AES chart (at wavelengths of 196.026 nm and 203.985 nm) are very close to or even overlap with those of Mn (196.025 nm) and Cr (203.991 nm), which is one of the reasons why the Se leaching concentration could not be measured accurately by the ICP-AES analysis.

In the two kinds of non-acidic leachates, the As leaching concentrations of GP mortar using WG solution were lower than the limits for the recycled materials used in contact with water except series 12-40-WG, but in the acidic leachate, the leaching concentrations were only below the limit for the recycled materials used without water contact. The Cr leaching in the alkaline water was not almost detected, but the Cr leaching concentrations in the acidic and neutral leachates depended on the used BA samples, which met the limit for the recycled materials used in contact with water, except series 23-40-WG, 8-40-WG, and 12-40-WG that used the 23/'19, 8/'19, 12/'19 BA samples, respectively. The Cr leaching from series 23-40-WG, 8-40-WG, and 12-40-WG in the acidic leachate only satisfied the limit for the recycled materials used without water contact.

The Pb leaching concentration in the neutral leachate was so low as to be undetectable, and the leaching concentration in the alkaline water was lower than the limit for the recycled materials used without water contact. However, in the acidic leachate, the Pb leaching was large, even comparable to that of the original BA sample used. In the ultrasonic oscillation method, the used GP mortar sample was 5 mm or less in dimension, which was the same to the maximum size of BA particles, thus the cutting section of large BA particle might be exposed directly to the leachate, resulting in a larger Pb leaching from the GP mortar than from the original BA used. Non-uniform distribution of Pb in BA samples may be another reason. The 12/'19 BA sample had more large particles than other BA samples, and larger BA particles contain more Pb (Loginova *et al.* 2019). Therefore, the Pb leaching concentration of series 12-40-WG was higher than that of the original BA samples discharged in other months but not in Dec. 2019.

That is to say, in neutral and alkaline environments, the leaching amount was lower than the limit of recycled construction materials used without water contact, regardless of the mixtures of GP mortar or the sort of trace

Table 12 Leaching concentration (mg/L) of trace elements in BFS/CFA-based GP mortars.

Element	pH of leachate	23-40 -WG	6-40 -WG	8-40 -WG	10-40 -WG-H	10-40 -WG-A	12-40 -WG	10-40 -11	10-40 -NH	10-70 -WG-H	10-70 -WG-A	10-100 -WG-H	10-100 -WG-A
Cr*	4.01	0.07	0.05	0.07	0.03	0.03	0.07	0.03	0.02	0.03	0.02	0.03	0.02
	6.86	0.03	0.03	0.03	0.03	0.03	0.03	0.03	0.03	0.03	0.03	0.03	0.03
	Water	ND	ND	0.01	ND	ND	ND	0.01	0.01	ND	ND	ND	ND
Cu	4.01	0.30	0.52	0.87	0.59	0.37	1.02	0.38	0.26	0.23	0.17	0.13	0.08
	6.86	0.01	0.02	0.03	0.03	0.03	0.02	0.02	0.01	0.03	0.01	0.01	0.01
	Water	0.01	0.01	0.07	0.03	0.05	0.01	0.18	0.06	0.03	0.02	0.06	0.01
Mn	4.01	0.34	0.38	0.52	0.40	0.37	0.50	0.46	0.56	0.46	0.38	0.44	0.42
	6.86	0.01	0.01	0.01	0.02	0.01	0.02	0.01	ND	0.02	ND	0.01	ND
	Water	ND	ND	0.03	0.01	0.01	ND	0.04	0.04	0.01	ND	0.02	ND
Pb	4.01	0.10	0.10	0.17	0.09	0.09	0.16	0.08	0.07	0.10	0.06	0.06	0.04
	6.86	ND	ND	ND	ND	ND	ND	ND	ND	ND	ND	ND	ND
	Water	ND	ND	0.02	0.01	ND	ND	0.03	0.03	0.01	ND	0.02	0.01
Zn	4.01	2.24	2.36	4.16	1.26	0.97	4.66	3.24	2.46	1.56	2.69	0.85	0.31
	6.86	0.01	0.14	0.02	0.02	0.01	0.02	0.02	0.01	0.03	ND	0.01	ND
	Water	0.01	0.03	0.13	0.03	0.05	0.02	0.19	0.13	0.05	0.01	0.07	0.01
As	4.01	0.02	0.03	0.03	0.02	0.02	0.06	0.03	0.03	0.02	0.01	0.02	0.02
	6.86	ND	0.01	ND	0.01	ND	0.03	0.02	0.02	0.01	ND	ND	ND
	Water	0.01	ND	ND	0.01	0.01	0.02	0.03	0.02	0.01	ND	0.01	ND
Cd	4.01	ND	ND	ND	ND	ND	ND	ND	ND	ND	ND	ND	ND
	6.86	ND	ND	ND	ND	ND	ND	ND	ND	ND	ND	ND	ND
	Water	ND	ND	ND	ND	ND	ND	ND	ND	ND	ND	ND	ND
Se	4.01	ND	ND	ND	ND	ND	ND	ND	ND	ND	ND	ND	ND
	6.86	ND	ND	ND	ND	ND	ND	ND	ND	ND	ND	ND	ND
	Water	ND	ND	ND	ND	ND	ND	ND	ND	ND	ND	ND	ND

[Notes] 1) ND means undetected due to exceeding the limit of the ICP-AES device.
2) Cr* is total amount of Cr (III) and Cr (VI).

Table 13 Results of standard leaching test (mg/L) for the BFS/CFA-based GP mortars.

Mixture	Cr	Cu	Mn	Pb	Zn	As	Cd	Se
10-40-WG-H	0.03 [d]	0.69	0.43	0.04	1.52	0.03	ND	ND
10-40-NH	0.01 [d]	0.07	0.25	0.01	1.93	0.04	ND	ND
Leaching limit [a]	0.05 [c]	None	None	0.01	None	0.01	0.01	0.01
Leaching limit [b]	0.15 [c]	None	None	0.03	None	0.03	0.03	0.03

[Notes] 1) ND means leaching concentration is too small to be detected.
2) *a* is leaching concentration limit for recycled construction materials used with contacting with water directly, *b* is leaching concentration limit for recycled construction materials used without water contact, *c* is environmental criteria value of Cr (VI), and *d* is total amount of Cr (III) and Cr (VI).

HMEs. However, in acidic environment, the leaching concentrations of Pb and As possibly exceeded the limits. By the way, through this leaching experiment, we realized that the test result of heavy metal leaching of GP materials with BA as fine aggregate is greatly influenced by two factors beside the accuracy of instrument: the distribution of HME in the BA used in GP, and the BA distribution in GP sample used for leaching analysis.

Table 13 shows the leaching concentrations of HMEs for series 10-40-WG-H and series 10-40-NH, which were cured by the heat-curing method and then stored for one year in the ambient air. The leaching concentrations were measured by the stirring method. The leaching concentrations of Cd, and Se were too small to be detected. Except for As and Pb, other HMEs' leaching concentrations were not over the limits for the recycled construction materials used without water contact.

The As leaching concentration of series 10-40-NH, and the Pb leaching concentration of series 10-40-WG-H were 0.04 mg/L, which was slightly larger than the leaching limit (0.03 mg/L) for recycled construction materials used without water contact. The BA was used as the whole of fine aggregate in this study. By substituting part of BA with natural sand, it is expected that the leaching limits of As and Pb (0.03 mg/L) would be satisfied.

Figure 13 shows the immobilization efficiency (IE) of HMEs, measured by the ultrasonic oscillation method. As explained above, the IE was an average of the upper and the lower limits of IE value because the moisture contents of GP mortar samples were not measured. In addition, the calculation of IE assumed that the HMEs of BA, CFA and BFS are soluble, thus the contents of HMEs measured by the XRF were used in the calculation. The IE values, gotten under the same conditions, can be used to compare the immobilization efficiencies of the same GP mortar in different leaching environments. From **Fig. 13**, it was found that the IE of each HME is 99.5% or more in the neutral and alkaline leachates. Even in the

acidic leachate, the fixation rate exceeded 97.9% except for Zn. Since the BA contained a large amount of Zn, the IE decreased slightly, but it was still higher than 96.5%.

It is considered that excellent HME immobilization of GP is attributed to the chemical immobilization of HMEs assimilated as charge-balancing elements, and the physical encapsulation of HMEs trapped into the 3-dimensional GP structure (Izquierdo *et al.* 2009). In neutral environment, the immobilization of Cr was relatively weak, which was consistent with the past study (Chen *et al.* 2016). It has been reported that Cr (VI) is much more leachable than Cr (III), thus it cannot be effectively immobilized in geopolymer (Zhang *et al.* 2008). The valence of Cr may change from Cr (III) in BA to Cr (VI) in the GP mortars. The addition of iron source, which exists as a hydroxy complex or precipitates as an oxy-

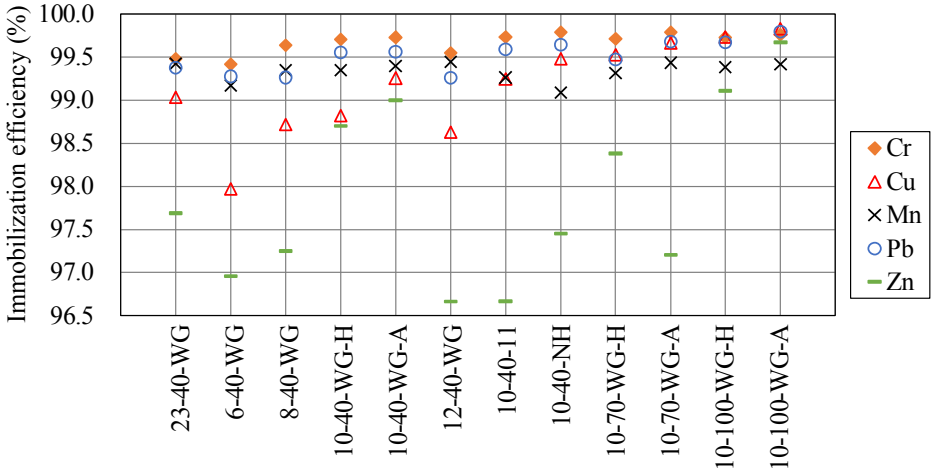

(a) In pH 4.01 leachate

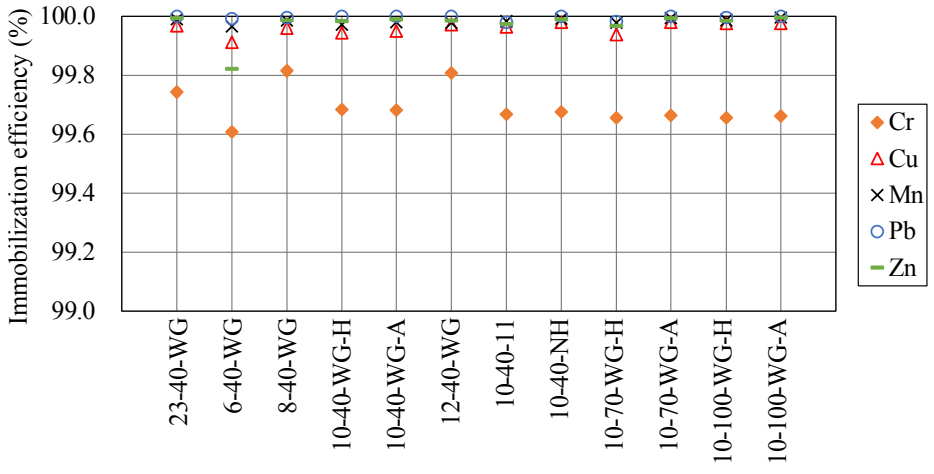

(b) In pH 6.86 leachate

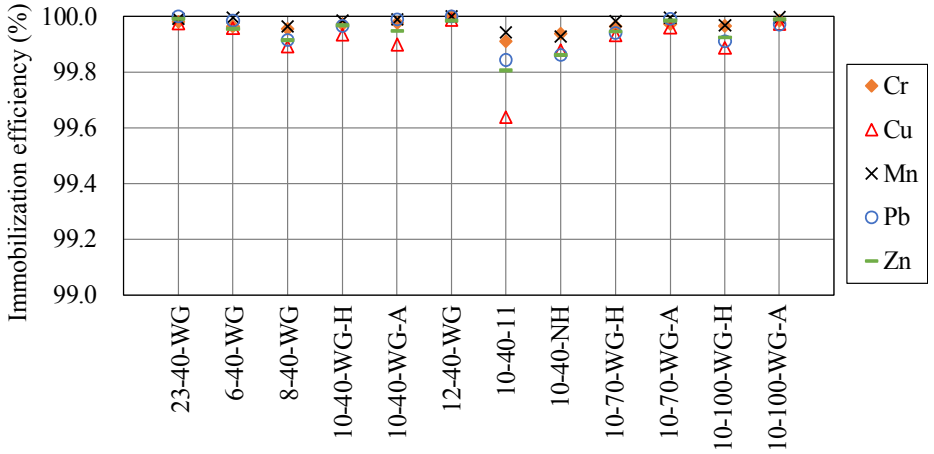

(c) In pure water (actually alkaline leachate)

Fig. 13 Immobilization efficiency of heavy metals of BFS/CFA-based geopolymer mortars.

hydroxide (goethite), can potentially improve the immobilization of As (Fernández-Jiménez *et al.* 2004).

4.5 Chemical and microstructural characterization

4.5.1 XRD results

Figure 14 shows the XRD patterns for four types of BFS/CFA-based geopolymer mortars, which used different AA solutions. The XRD patterns of the used BA and coal fly ash (CFA) are also shown in **Fig. 14**, but BFS is omitted because there is no crystal phase. The four GP mortars had almost the same crystal phases with those contained in BA and CFA. The mullite in the CFA was not found in the GPs. This is due to the small mullite content in the CFA and the small CFA content in the GP mortars. The C4 disappeared in series of 10-40-WG-H, 10-40-11, and 10-40-NH, but still remained in series of 23-40-WG. This is because there was too much C4 in the 23/'19 BA sample, which was not completely dissolved. The calcite peak is so low that almost not be observed in series 10-40-NH, suggesting that $CaCO_3$ would be dissolve in highly alkaline solution. Series 23-40-WG and 10-40-WG using WG as AA solution had very small amount of anorthite, of which the reason is not clear now. In addition, anhydrite was observed in the GPs, indicating that it is embedded in BA particles so as not to react easily with WG solution, In the 2θ range of 25-35 degrees, the XRD patterns show broad humps, indicating that amorphous phases were formed. As discussed later, these amorphous components were mainly C-A-S-H gels.

4.5.2 SEM-EDS results

Figure 15 shows SEM images of two series of BFS/CFA-based GP mortars using BA as fine aggregate, in which either WG or NH solution was used as AA solution. It was found from images (1) and (4) of **Fig. 15** that in the two mortars, there were many BA particles with many pores inside, which indicates that BA particles are porous and irregular, and the GP using the NH solution had many large cracks and was less dense than the GP using the WG solution. However, fine cracks were found in series 10-40-WG [see SEM image (3) of **Fig. 15**], which were generally caused by dry shrinkage. One effective solution to reduce the drying shrinkage is to add the shrinkage reducer that was developed for GP materials (Okada *et al.* 2017). In addition, many incompletely reacted CFA particles were clearly observed in the two mortars. As shown in SEM images (3) and (7) of **Fig. 15**, series 10-40-WG had denser GP matrices than series 10-40-NH. From the SEM images (5), (6), (8), and (9) of **Fig. 15**, we found that in the GP using the NH solution, there were a lot of granulated crystals and rod-shaped crystals with 1-2 μm size and rough surface. The discontinuous distribution of granulated crystals may be one of the reasons why the strength of series 10-40-NH was lower than that of series 10-40-WG.

EDS point analyses were further performed for the 23 spots marked in the SEM images (3) and (6) to (9) of **Fig. 15**. The results are shown in the **Table 14**. The reaction products of series 10-40-WG were almost C-A-S-H gels. However, in the series 10-40-NH, the N-A-S-H gels were also detected besides the C-A-S-H gels. Both the granulated crystals and the plat matrices in SEM image (8) of **Fig. 15**, as well as spots 7 and 8 in **Fig. 15**, image (6), had the compositions of C-A-S-H. The pit in image (6) of **Fig. 15** was a trace left after the CFA particle was separated,

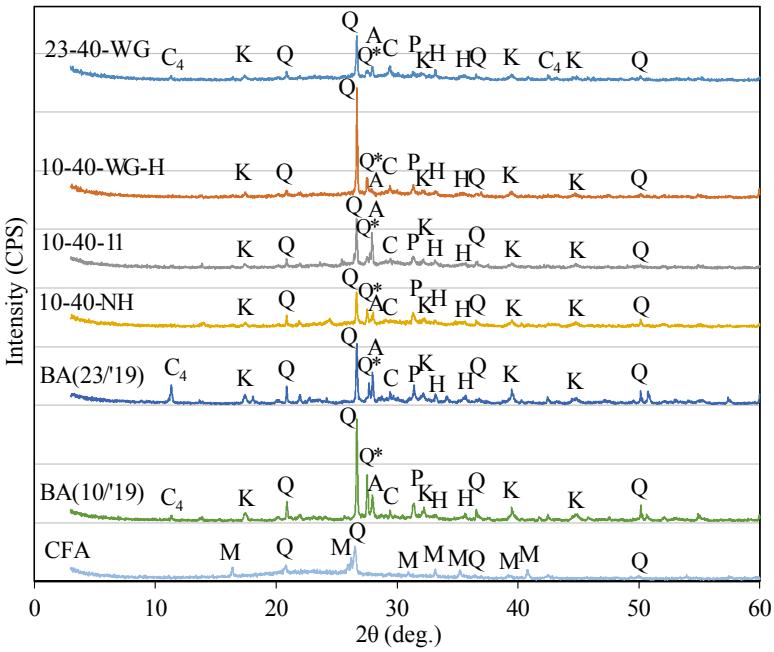

[Notes] Q: Quartz, SiO_2; Q*: Quartz-HP, SiO_2; C: Calcite, $CaCO_3$; A: Anorthite, $CaAl_2Si_2O_8$; K: Katoite, $Ca_3Al_2(OH)_{12}$; H: Hematite, Fe_2O_3; P: Anhydrite, $CaSO_4$; C_4: Hydrotalcite, $Ca_4Al_2O_6Cl_2{\cdot}10H_2O$; M: Mullite, $3Al_2O_3{\cdot}2SiO_2$.

Fig. 14 XRD patterns of BFS/CFA-based geopolymer mortars using BA as fine aggregate.

and the rod-shaped crystals in the pit should be intact mullite left by the dissolved CFA particle from the shape and size of the crystals. In addition, the particles in clusters shown in image (9) of **Fig. 15** had the compositions of N-A-S-H, which were crystallized N-A-S-H gels. As discussed in Section 3.2 2, the crystallized N-A-S-H gels changed as three-dimensionally bonded gobbinsite particles, a kind of zeolite. It is considered that the formation of N-A-S-H gels in series 10-40-NH was attributed to the high leaching of Al^{3+} from the precursors, especially coal fly ash, and the metallic aluminum in BA may be another Al^{3+} source under the high alkalinity of NaOH. As shown in **Fig. 7**, gobbinsite was found in the GP using BA as sole precursor. At present, the reasons for the crystallization of C-A-S-H/N-A-S-H gels and the formation of gobbinsite are unknown. BA is alkaline (pH>12.0) since it contains free CaO or $Ca(OH)_2$ derived from limestone, which is used in incinerators to prevent flue gas pollution. Thus, we speculate that excessively high alkalinity due to the use of NH may be one of reasons and further investigation is needed.

5. Conclusions

In this study, in order to develop a new technology for safely recycling municipal solid waste incineration bottom ash (BA), the properties, chemical components and micro-structure of geopolymer (GP) using BA as precursor or as fine aggregate were investigated in detail, and the effects of mixture, curing method, and BA's discharge time were discussed. The leaching behaviors of heavy metals of GP mortars in the environments with different pH values were examined. The mortars used ground granulated blast furnace slag (BFS) and coal fly ash (CFA) as precursors, and used the BA as fine aggregate. Obtained main results are summarized as follows.

1) The chemical compositions of BA varied with its discharge time. The BAs, which were discharged in cold season (Dec.-Feb.), contained more CaO and chlorine, but less SiO_2. Conversely, the BAs discharged in warm season (May-Oct.) had less CaO and chlorine, but more SiO_2. The Al_2O_3 contents in the BA samples were almost unchanged with BA's discharge time. Na_2O and K_2O contents are highest in

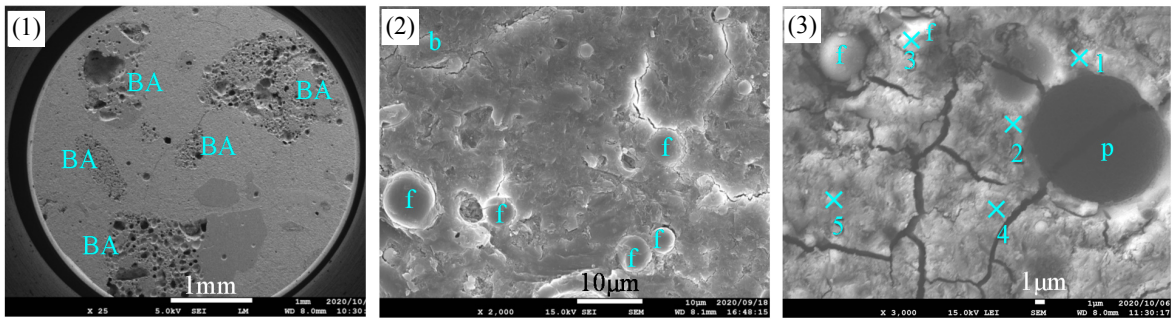

(a) Series 10-40-WG. The magnifications of the images are: (1) 25, (2) 2000 and (3) 3000.

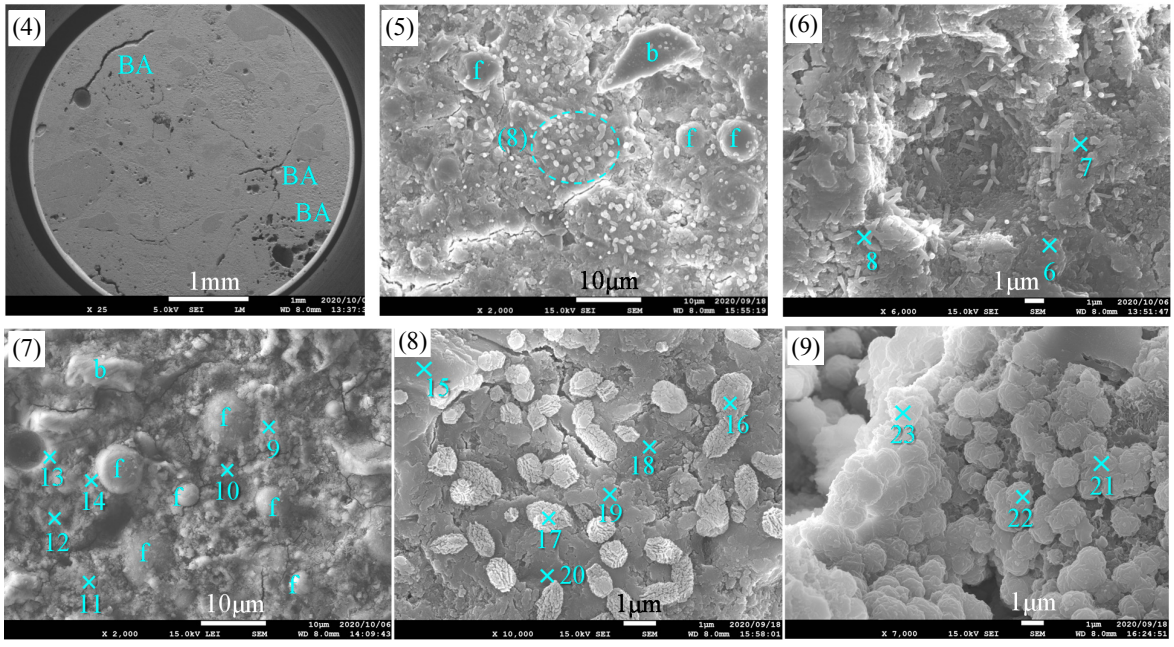

(b) Series 10-40-NH. The magnifications of the images are: (4) 25, (5) 2000, (6) 6000, (7) 2000, (8) 10 000 and (9) 7000.

Fig. 15 SEM images of BFS/CFA-based GP mortars using BA as fine aggregate (b: BFS particle, f: CFA particle, p: Pore).

Table 14 Results of SEM-EDS point-analysis for series 10-40-WG and series 10-40-NH.

Spot	Mole percentage of oxide and chloride (%)											(C+M)/(N+K)*	(Al+Si)/(Na+Ca+K)**	Compound
	SiO_2	TiO_2	Al_2O_3	Fe_2O_3	CaO	MgO	Na_2O	K_2O	P_2O_5	SO_3	Cl			
1	23.36	0.84	14.59	0.79	50.45	6.46	0.81	0.00	0.00	2.69	0.00	70.46	1.01	C-A-S-H
2	35.95	0.00	7.44	0.00	46.56	3.75	3.98	0.00	0.00	2.33	0.00	12.66	0.93	C-A-S-H
3	83.48	0.71	9.09	0.00	2.60	1.84	1.63	0.65	0.00	0.00	0.00	1.94	14.20	CFA particle
4	34.51	0.00	13.10	0.00	47.66	2.71	2.02	0.00	0.00	0.00	0.00	24.93	1.17	C-A-S-H
5	55.10	0.57	17.42	4.12	13.06	5.13	2.43	0.63	0.00	1.53	0.00	5.94	4.69	C-A-S-H
6	55.56	0.00	32.32	0.00	4.19	0.00	5.97	0.69	0.00	1.27	0.00	0.63	6.86	N-A-S-H
7	10.62	0.00	1.93	0.00	57.48	2.11	8.74	0.00	18.74	0.00	0.39	6.82	0.19	C-A-S-H
8	47.18	0.00	6.73	1.49	34.17	3.51	4.34	0.68	0.00	1.90	0.00	7.51	1.37	C-A-S-H
9	60.56	0.00	7.44	1.53	16.38	3.88	7.49	1.01	0.00	1.26	0.47	2.38	2.26	C-A-S-H
10	49.66	0.00	27.08	1.46	10.10	2.44	6.67	0.47	0.00	1.46	0.66	1.76	4.26	C-A-S-H
11	53.66	0.44	12.44	2.64	12.68	5.55	9.11	0.75	0.00	1.74	0.99	1.85	2.42	C-A-S-H
12	55.96	0.58	4.66	1.27	23.84	4.81	6.59	0.83	0.00	1.46	0.00	3.86	1.69	C-A-S-H
13	49.38	1.46	18.50	3.48	12.47	4.70	9.27	0.73	0.00	0.00	0.00	1.72	2.66	C-A-S-H
14	62.05	0.68	11.85	2.30	9.33	2.21	8.65	1.27	0.00	0.98	0.68	1.16	2.94	C-A-S-H
15	36.93	0.00	7.93	0.00	44.32	7.24	1.02	0.00	0.00	2.57	0.00	50.39	1.14	C-A-S-H
16	41.83	0.00	5.88	0.00	41.66	4.37	4.28	0.55	0.00	1.43	0.00	9.52	1.04	C-A-S-H
17	44.70	0.00	8.79	0.00	34.30	4.45	5.10	0.58	0.00	2.08	0.00	6.83	1.36	C-A-S-H
18	54.59	0.00	4.82	1.03	28.94	4.55	3.96	0.69	0.00	1.42	0.00	7.21	1.68	C-A-S-H
19	57.30	0.41	8.49	1.54	18.51	6.79	4.91	0.72	0.00	1.33	0.00	4.50	2.50	C-A-S-H
20	51.10	0.53	12.00	1.22	23.65	2.70	6.23	0.62	0.00	1.20	0.75	3.85	2.01	C-A-S-H
21	55.81	0.00	21.12	0.00	7.20	1.91	12.51	1.45	0.00	0.00	0.00	0.65	2.79	Gobbinsite
22	55.22	0.00	21.27	0.00	5.76	2.06	14.00	1.68	0.00	0.00	0.00	0.50	2.63	Gobbinsite
23	58.00	0.00	16.62	1.78	7.71	0.99	11.97	2.30	0.00	0.00	0.63	0.61	2.52	Gobbinsite

[Notes] 1) * obtained from the molar percentages of metal oxides.
2) ** obtained from the molar percentages of metal elements.

BA discharged in Aug.-Oct. However, there are no certain patterns in the effects of the discharge time of BA on its heavy metal content and crystalline phase type. The crystalline phases were mainly quartz, calcite, anorthite, katoite, hematite, and hydrotalcite ($Ca_4Al_2O_6Cl_2 \cdot 10H_2O$). In the GP, the hydrotalcite reacted and almost disappeared. Cr, Cu, Pb, Zn contents were large, but As and Se contents in the BA samples were below the XRF analysis limits. Moreover, density and particle size distribution of BA also varied with its discharge time. The density of BA discharged in August-October was larger, but the particles were slightly finer, compared to the BA discharged in the cold season.

2) The GP monolith using only BA as precursor had a low strength due to locally or entirely porous structure. BA has a low reactivity of polymerization reaction so as to be more suitable to be recycled as fine aggregate of GP materials, rather than GP precursor.
3) BFS/CFA-based GP mortars, using only sodium silicate (WG) as AA solution, had larger strength and longer setting time, compared to the GP mortars using the AA solution containing sodium hydroxide (NH). The GP mortar with NH was not dense, which locally contained the crystallized C-A-S-H and N-A-S-H gels, being gobbinsite. Like as the GP mortar using natural sand, the larger the BFS content, the greater the strength and the carbonation resistance of GP mortar with BA as fine aggregate, and the heat-curing yielded higher strength and carbonation resistance than the ambient curing. The GPs using the BAs discharged in Aug.-Oct. had a greater strength than using the BAs discharged in the cold season. The products of the BFS/CFA-based GP mortars using WG as AA solution were mainly C-A-S-H gels.
4) The heavy metal elements contained in BA varied with its discharge times. The lower the pH of leachate, the higher the amount of leaching from the BA samples regardless of trace elements. The leaching of Cr, Cu, Mn, and Zn was relatively high, but Pb and Cd leaching was detected only in the acidic leachate for some BA samples, and Se leaching was not detected in the three leachates for all the BA samples.
5) The leaching of heavy metal elements from BFS/CFA-based GP mortar using BA depended on the leaching environment (pH value), BA's discharge time, and mixture of GP mortar. The lower the pH of leachate, the greater the leaching concentration. The more the heavy metals in BA sample, the more the leaching from GP mortar with the BA sample. The effects of BFS content in precursors and curing method on the leaching depended on the sort of heavy metal element. For the same GP mortar, the effect of BA's discharge time was not found in this experiment. The leaching concentrations of almost all trace toxic elements of the GP mortars even in the acidic water were lower than the limits for the recycled construction materials used without water contact, whereas the leaching concentrations of Pb and As in acidic water were above limits for the recycled construction materials used in contact with water. Therefore, GP materials

using BA can be used without direct contact with water or in non-acidic water environment, however, when used in acidic water environment, BA content must be reduced by blending other harmless fine aggregate.

Acknowledgments

We would like to thank Sanko Holdings Co., Ltd. for providing financial support for this research, and Mr. K. Shooji and Mr. H. Satou, employees of Sanko Holdings, for their experimental collaboration.

References

Arbi, K., Nedeljković, M., Zuo, Y. and Ye, G., (2016). "A review on the durability of alkali-activated fly ash/slag systems: Advances, issues, and perspectives." *Industrial & Engineering Chemistry Research*, 55, 5439-5453.

Arickx, S., De Borger, V., Van Gerven, T. and Vandecasteele, C., (2010). "Effect of carbonation on the leaching of organic carbon and of copper from MSWI bottom ash." *Waste Management*, 30, 1296-1302.

Bernal, S. A. and Provis, J. L., (2013). "Gel nanostructure in alkali-activated binders based on slag and fly ash, and effects of accelerated carbonation." *Cement and Concrete Research*, 53, 127-144.

Chen, Z., Liu, Y., Zhu, W. and Yang, E., (2016). "Incinerator bottom ash (BA) aerated geopolymer." *Construction and Building Materials*, 112, 1025-1031.

Davidovits, J., (2015). "*Geopolymer chemistry and applications*." Saint-Quentin, France: Institut Géopolymère.

Feng, D., Mikuni, A., Hirano, Y., Komatsu, R. and Ikeda, K., (2005). "Preparation of geopolymeric material from fly ash filler by stream curing with special reference to binder products." *Journal of the Ceramic Society of Japan*, 113, 82-86.

Fernández-Jiménez, A. M., Lachowski, E. E., Palomo, A. and Macphee, D. E., (2004). "Microstructural characterisation of alkali-activated PFA matrices for waste immobilisation." *Cement and Concrete Composites*, 26(8), 1001-1006.

Gao, X., Yuan, B., Yu, Q. L. and Brouwers, H. J. H., (2017). "Characterization and application of municipal solid waste incineration (MSWI) bottom ash and waste granite powder in alkali activated slag." *Journal of Cleaner Production*, 164, 410-419.

Giro-Paloma, J., Ribas-Manero, V., Maldonado-Alameda, A., Formosa, J. and Chimenos, J. M., (2017). "Use of municipal solid waste incineration bottom ash and crop by-product for producing lightweight aggregate." *Materials Science and Engineering*, 251, Article ID 012126.

Hjelmar, O., (1996). "Disposal strategies for municipal solid waste incineration residues." *Journal of Hazardous Materials*, 47, 345-368.

Ikeda, S., Ishikawa, T., Harada, S. and Kikuchi, M., (2009). "Evaluation of the safety of concrete using molten slag fine aggregate." *Proceedings of the Japan Concrete Institute*, 31, 805-810 (in Japanese)

Izquierdo, M., Querol, X., Davidovits, J., Antenucci, D., Nugteren, H. and Fernández-Pereira, C., (2009). "Coal fly ash-slag-based geopolymers: Microstructure and metal leaching." *Journal of Hazardous Materials*, 166, 561-566.

JCI, (2017). "*Report of the research committee on the application of geopolymer technology to construction field*." Tokyo: Japan Concrete Institute. (in Japanese)

Jo, B. W., Kim, K. I., Park, J. C. and Park, S. K., (2006). "Properties of chemically activated MSWI (municipal solid waste incinerator) mortar." *Journal of the Korea Concrete Institute*, 18, 589-594.

JSCE, (2003). "*Leaching of minor elements from concrete* (Concrete Library No. 111)." Tokyo: Japan Society of Civil Engineers. (in Japanese)

Kamada, Y., (2016). "*Study on the separation and recycling of heavy metals and alkali metals by melting process*." Thesis (PhD). Okayama University. (in Japanese)

Kondo, R., Li, Z. and Kim, H., (2020). "Study on organic compound emissions from geopolymer mixing with municipal waste incineration ash." *Summaries of Technical papers of Annual Meeting, Architectural Institute Japan*, 1147-1148. (in Japanese)

Kondo, R., Li, Z. and Ikeda, K., (2020). "Recycling and heavy metal immobilization of waste incineration ash by geopolymer production" In: *Proceedings of ConMat'20, The 6th International Conference on Concrete Materials - Performance, Innovations, and Structural Implications*, Fukuoka, Japan 27-29 August 2020. Tokyo: Japan Concrete Institute, Paper No. 3-2_2, 877-886.

Kuo, W. T., Liu, C.-C. and Su, D. S., (2013). "Use of washed municipal solid waste incinerator bottom ash in pervious concrete." *Cement and Concrete Composites*, 37, 328-335.

Lee, W. K. and Son, Y. G., (2012). "Effect on the compressive strength of pastes made from MSWI bottom ash with mixing ratio of sodium silicate and potassium silicate." *Journal of Korea Society of Waste Management*, 29, 93-97.

Li, Z., (2016a). "Assessment of the environmental impact of geopolymer concrete." In: *Proceedings of the Symposium on Current Status and Issues of Geopolymer Technology in Construction*, Tokyo 24 June 2016. Tokyo: Japan Concrete Institute, 43-50. (in Japanese)

Li, Z., (2016b). "Geopolymer and practical application in construction materials, Part 2: Raw materials used and status of application." *Journal of the Japan Testing Center for Construction Materials*, 52, 2-7. (in Japanese)

Li, Z. and Ikeda, K., (2018). "*Foaming geopolymer using ground waste incineration slag*." Japanese Patent No. 6430268. (in Japanese)

Li, Z., Ikeda, K. and Zhang, Y., (2013). "Development of geopolymer concrete using ground molten slag of municipal waste incineration ash." In: *Proceedings of 3rd International Conference on Sustainable Construction Materials and Technologies*, Kyoto 18-21 August

2013. Tokyo: Japan Concrete Institute, 71-78.

Li, Z. and Ikeda, K., (2019). "Application of preheating treatment to setting control of geopolymer cement using ground granulated blast furnace slag." In: *Proceedings of 15th International Congress on the Chemistry of Cement*, Prague 16-19 September 2019, Paper No. 507.

Li, Z. and Li, S., (2018). "Carbonation resistance of fly ash and blast furnace slag based geopolymer concrete." *Construction and Building Materials*, 163, 668-680.

Li, Z. and Li, S., (2020). "Effects of wetting and drying on alkalinity and strength of fly ash/slag-activated materials." *Construction and Building Materials*, 254, Article ID 119069.

Li, Z., Nagashima, M. and Ikeda, K., (2018). "Treatment technology of hazardous water contaminated with radioisotopes with paper sludge ash-based geopolymer ― Stabilization of immobilization of strontium and cesium by mixing seawater." *Materials*, 11(1521), 1-21.

Loginova, E., Volkov, D. S., van de Wouw, P. M. F., Florea, M. V. A. and Brouwers, H. J. H., (2019). "Detailed characterization of particle size fractions of municipal solid waste incineration bottom ash." *Journal of Cleaner Production*, 207, 866-874.

Maldonado-Alameda, A., Giro-Paloma, J., Svobodova-Sedlackova, A., Formosa, J. and Chimenos, J. M., (2020). "Municipal solid waste incineration bottom ash as alkali-activated cement precursor depending on particle size." *Journal of Cleaner Production*, 242, Article ID 118443.

MEJ, (2020). "*Annual report on the status of general waste emissions and treatment (Fiscal year 2018)*." Tokyo: Ministry of the Environment of Japan. (in Japanese)

Okada, T., Li, Z., Hashizume, S. and Nagai, T., (2017). "A study on the effects of shrinkage reducing agent on the performances of geopolymer concrete using fly ash and ground granulated blast furnace slag." *Proceedings of the Japan Concrete Institute*, 39, 2029-2034. (in Japanese)

Palomo, Á., Alonso, A. and Fernández-Jiménez, A. M., (2004). "Alkaline activation of fly ashes: NMR study of the reaction products." *Journal of the American Ceramic Society*, 87, 1141-1145.

Sakanakura, H., (2019). "*Recycling of general waste incineration ash - Significance and issues*." Public Research Presentation, Tokyo Metropolitan Research Institute for Environmental Protection. (in Japanese)

TMEB, (2009). "*Simple and rapid analysis method for heavy metals in soil (pretreatment with ultrasound)*." Tokyo: Tokyo Metropolitan Environment Bureau. (in Japanese)

Tome, S., Etoh, M.-A., Etame, J. and Sanjay, K., (2018). "Characterization and leachability behaviour of geopolymer cement synthesised from municipal solid waste incinerator fly ash and volcanic ash blends." *Recycling*, 3(4), Article ID 3040050.

Vempati, R. K., Mollah, M. Y. A., Chinthala, A. K., Cocke, D. L. and Beeghly, J. H., (1995). "Solidification/ stabilization of toxic metal wastes using coke and coal combustion by-products." *Waste Management*, 15, 433-440.

Yamaguchi, N., Nagaishi, M., Kisu, K., Nakamura, Y. and Ikeda, K., (2013). "Preparation of monolithic geopolymer materials from urban waste incineration slags." *Journal of the Ceramic Society of Japan*, 121, 847-854.

Zhang, J., Provis, J. L., Feng, D. and van Deventer, J. S. J., (2008). "Geopolymers for immobilization of Cr^{6+}, Cd^{2+}, and Pb^{2+}." *Journal of Hazardous Materials*, 157, 587-598.

Zhang, Z., Provis, J. L. and Wang, H., (2015). "Critical thinking on efflorescence in alkali activated cement (AAC)." In: D. Fernando, J.-G. Teng and J. L. Torero, Eds. *Proceedings of the 2nd International Conference on Performance-Based and Life cycle Structural Engineering*, Brisbane, Australia 9-11 December 2015. Queensland: University of Queensland, 147-153.

Zhu, W., Chen, X., Struble, L. J and Yang, E.-H., (2016). "Feasibility study of municipal solid waste incinerator bottom ash as geopolymer precursor." In: N. Ghafoori, P. Claisse and E. Ganjian, Eds. *Proceedings of 4th International Conference on Sustainable Construction Materials and Technologies*, Las Vegas, USA 7-11 August 2016. UK: Coventry University, Paper No. S190.